

**PHOTOCATALYTIC DEGRADATION OF HUMIC ACID
IN A WATER ENVIRONMENT**

BY

PUTRI ARDYARINI SEKARTAJI

**A THESIS SUBMITTED IN PARTIAL FULFILLMENT OF THE
REQUIREMENTS FOR THE DEGREE OF MASTER OF SCIENCE
(ENGINEERING AND TECHNOLOGY)
SIRINDHORN INTERNATIONAL INSTITUTE OF TECHNOLOGY
THAMMASAT UNIVERSITY
ACADEMIC YEAR 2015**

**PHOTOCATALYTIC DEGRADATION OF HUMIC ACID
IN A WATER ENVIRONMENT**

BY

PUTRI ARDYARINI SEKARTAJI

**A THESIS SUBMITTED IN PARTIAL FULFILLMENT OF THE
REQUIREMENTS FOR THE DEGREE OF MASTER OF SCIENCE
(ENGINEERING AND TECHNOLOGY)
SIRINDHORN INTERNATIONAL INSTITUTE OF TECHNOLOGY
THAMMASAT UNIVERSITY
ACADEMIC YEAR 2015**



PHOTOCATALYTIC DEGRADATION OF HUMIC ACID IN A WATER
ENVIRONMENT

A Thesis Presented

By

PUTRI ARDYARINI SEKARTAJI

Submitted to

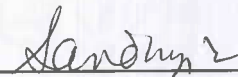
Sirindhorn International Institute of Technology

Thammasat University

In partial fulfillment of the requirements for the degree of
MASTER OF SCIENCE (ENGINEERING AND TECHNOLOGY)

Approved as to style and content by

Advisor and Chairperson of Thesis Committee



(Assoc. Prof. Dr. Sandhya Babel)

Committee Member and
Chairperson of Examination Committee



(Assoc. Prof. Dr. Alice Sharp)

Committee Member



(Assoc. Prof. Dr. Patiparn Punyapalukul)

May 2016

Acknowledgements

First and foremost I offer my sincerest gratitude to my supervisor, Assoc. Prof. Dr. Sandhya Babel, who has supported me through out my research and writing the thesis with her precious guidance. One simply could not wish for a better or friendlier supervisor in SIIT, Thammasat University.

Besides my supervisor, I personally would like to thank you to Assoc. Prof. Dr. Alice Sharp as internal committee member and Assoc. Prof. Dr. Patiparn Punyapalakul as external committee member, for their encouragement, insightful comments, and precious suggestions.

I would also like to express my appreciation to Asst. Prof. Dr. Paiboon Sreearunothai for generously provide the raw materials required to support my research work. I would like to thank to Mrs. Charinnarat Mongkolthalang as a coordinator of ADB scholarship for helping me during study, regarding the scholarship service. Particular thanks are given to all staffs of the Bio-Chemical Engineering and Technology of SIIT for their kind help and support.

I further extend my personal gratitude to Asst. Prof. On-anong Larpparisudthi, Ph.D (Chulalongkorn University) for her considerable expertise, valuable discussion and suggestions. I would like to thank to Mr. Surawut Protatokung Siratham, a person who is very helpful and kindness to teach me during the TOC analysis at Environmental Engineering Laboratories, Chulalongkorn University. My sincere thanks also goes to Mr. Hanggara Sudrajat for sharing his valuable knowledge and fruitful discussions.

I would like to gratefully thank to the Japanese Government, which was through the ADB (Asian Development Bank), awarded me the greatly prestigious ADB-JSP scholarship for pursuing and accomplishing master degree at SIIT.

Most important above all, I am sincere gratitude to Almighty Allah for giving me the strengths and courage to overcome all the difficulties that I have faced throughout my life so far.

Finally, I thank my parents and family for continuously supporting, loving, caring and encouraging me throughout all my studies at SIIT. And last but not least, I thank to my best friends for always being there for me through good times and bad, until finally we accomplished this master together.

Abstract

PHOTOCATALYTIC DEGRADATION OF HUMIC ACID IN A WATER ENVIRONMENT

by

PUTRI ARDYARINI SEKARTAJI

Bachelor of Engineering in Environmental Engineering, Trisakti University, 2012

Humic acid (HA) is a well-known complex organic compound which can generate disinfection by-product which are harmful for health when contacted with chlorine during the drinking water treatment. The photocatalysis is a compromise alternative solution for the HA degradation in a water environment.

In this study, the degradation of HA, using titanium dioxide (TiO_2) and zinc oxide (ZnO) nanoparticles, irradiated by ultraviolet light, is investigated. The optimum conditions of pertinent factors, which include the light wavelength (UV-A and UV-C), and light intensity, HA concentration, catalyst dose, and contact time were investigated at neutral pH conditions, considered for drinking water treatment. Kinetics Langmuir-Hinshelwood are used to understand adsorption mechanisms and kinetics of HA degradation.

In terms of the HA degradation efficiency, ZnO had higher HA degradation efficiency compared to TiO_2 . In the short contact time 30 min to 60 min, it was reached more than 90%. Moreover, ZnO photocatalyst proved to be more compatible with UV-A light, whereas, TiO_2 with UV-C. Kinetics Langmuir-Hinshelwood was indicated that for both photocatalyst, under UV-A and UV-C irradiation followed a pseudo first order kinetic expression. The reusability of catalyst was performed and still revealed effective for beneficial commercial applications.

Keywords: *Humic Acid, Photocatalysis, ZnO, TiO_2 , UV Irradiation*

Table of Contents

Chapter	Title	Page
	Signature Page	i
	Acknowledgements	ii
	Abstract	iii
	Table of Contents	iv
	List of Figures	v
	List of Tables	vi
1	Introduction	1
	1.1 Background and Rationale	1
	1.2 Objectives of study	3
	1.3 Scope of study	3
2	Literature Review	5
	2.1 Humic Acids	5
	2.1.1 Definition of Humic Substances	6
	2.1.2 Classification of Humic Substances	6
	2.1.3 Definition of Humic Acid	7
	2.1.4 Source of Humic Acid	8
	2.1.5 Chemical Structure of Humic Acid	8
	2.1.6 Impact of Humic Acid Pollution on Organism and Environment	9
	2.2 Measurement of Humic Acid in a Water Environment	10
	2.3 Methods for Humic Acid Treatment	11
	2.4 Photocatalyst Degradation of Humic Acid	14
	2.4.1 Photocatalyst	14
	2.4.2 Photocatalysis	14
	2.4.3 Mechanism of Photocatalysis	15

2.4.4	Parameters Affecting The Photocatalytic Degradation	16
2.4.5	The kinetics of photocatalysis	17
3	Methodology	18
3.1	Materials and Methods	18
3.1.1	Preparation of synthetic of HA solution	18
3.1.2	Titanium dioxide (TiO ₂) as catalyst	18
3.1.3	Zinc oxide (ZnO) as catalyst	19
3.2	Experimental Equipment and Procedure	19
3.2.1	Experimental Equipment	19
3.2.2	Experimental Procedure	19
3.2.2.1	Photocatalytic Reactor	20
3.2.2.2	HA Analysis Method	22
3.3	Batch Experiments	22
3.3.1	Effect of catalyst dose	23
3.3.2	Effect of HA concentration	23
3.3.3	Effect of contact time	23
3.3.4	Effect of wavelength	23
3.3.5	Effect of Light Intensity	24
3.3.6	Catalyst Reusability	24
3.3.7	The kinetics of photocatalytic degradation	24
3.3.8	Characterization of catalyst	25
3.3.8.1	XRD Analysis	25
3.3.8.2	BET Analysis	26
3.3.8.3	FT-IR Analysis	26
3.3.8.4	XRF Analysis	26
3.3.8.1	TOC Analysis	26
4	Results and Discussions	27
4.1	HA Degradation by ZnO Photocatalyst	27

4.1.1	Characteristic of ZnO as a catalyst	27
4.1.1.1	XRD Analysis	27
4.1.1.2	FT-IR Analysis	28
4.1.1.3	BET Analysis	29
4.1.1.4	XRF Analysis	30
4.1.2	Pertinent factors of HA degradation	30
4.1.2.1	Effect of HA concentration	30
4.1.2.2	Effect of ZnO dose	32
4.1.2.3	Effect of contact time	33
4.1.2.4	Effect of light intensity	35
4.1.3	Adsorption isotherm	37
4.1.4	Reusability of catalyst	38
4.2	HA Degradation by TiO ₂ Photocatalyst	39
4.2.1	Characteristic of TiO ₂ as a catalyst	39
4.2.1.1	XRD Analysis	39
4.2.1.2	FT-IR Analysis	40
4.2.1.3	BET Analysis	42
4.2.1.4	XRF Analysis	42
4.2.2	Pertinent factors of HA degradation	43
4.2.2.1	Effect of HA concentration	43
4.2.2.2	Effect of TiO ₂ dose	44
4.2.2.3	Effect of contact time	45
4.2.2.4	Effect of light intensity	47
4.2.3	Adsorption isotherm	49
4.2.4	Reusability of catalyst	50
4.3	Pseudo-first order kinetics	51
4.3.1	Half-life ($t_{1/2}$)	56
4.3.2	Total Organic Carbon (TOC) and Mineralization	57
5	Conclusions and Recommendations	60
5.1	Conclusions	60

5.1.1 HA Degradation by ZnO Photocatalyst	60
5.1.2 HA Degradation by TiO ₂ Photocatalyst	60
5.1.3 Comparison of ZnO and TiO ₂ Photocatalyst	61
5.2 Recommendations	62
References	64
Appendices	69
Appendix A	70
Appendix B	71
Appendix C	72
Appendix D	75
Appendix E	78
Appendix F	79
Appendix G	83
Appendix H	86

List of Tables

Tables	Page
2.1 Major types of Humic Substance characterized by differences in solubility	6
2.2 The distribution of organic compounds in natural water	8
2.3 Environmental issues involving HS	10
2.4 The comparison of technologies to remove Humic Acid	12
3.1 Parameter and equipment used	19
4.1 Properties of ZnO based on BET analysis	30
4.2 ZnO elements based on XRF analysis	19
4.3 Properties of TiO ₂ based on BET analysis	42
4.4 TiO ₂ elements based on XRF analysis	43
4.5 Kinetic parameters of HA degradation by TiO ₂ photocatalyst at various initial HA concentration	54
4.6 Kinetic parameters of HA degradation by ZnO photocatalyst at various initial HA concentration	56
4.7 The percentage of TOC degradation efficiency	59

List of Figures

Figures	Page
2.1 Schematic representation of humic substances in dependence of their solubility	6
2.2 Properties of Humic Substances	7
2.3 Chemical Structure of Humic Acid	9
2.4 Mechanism of photocatalytic process and the reactions that occur at the surface	20
3.1 Overview of the batch photocatalytic degradation of HA	20
3.2 Schematic of the photocatalytic reactor	21
3.3 HA Analysis Methods	22
4.1 X-ray diffraction pattern of ZnO	27
4.2 FT-IR spectra of ZnO	29
4.3 Effect of HA concentration on degradation by ZnO photocatalyst (ZnO dose 0.1 g/L, contact time 60min)	31
4.4 Effect of ZnO dose on degradation of HA (HA conc. 5 mg/L, contact time 60 min)	32
4.5 Effect of contact time on degradation of HA by ZnO photocatalyst, (a)HA conc. 5 mg/L, ZnO dose 0.3 g/L, (b) HA conc. 14 mg/L, ZnO dose 0.3 g/L	34
4.6 Effect of light intensity on degradation of HA by ZnO photocatalyst, (a)HA conc. 5 mg/L, ZnO dose 0.3 g/L, contact time from 30 – 180 min, (b) UV-C, HA conc. 14 mg/L, ZnO dose 0.3 g/L, contact time from 30 – 180 min	36
4.7 The percentage of adsorption and photodegradation under UV-A and UV-C irradiation at different time	37
4.8 Catalyst reusability under UV-A and UV-C irradiation	39
4.9 X-ray diffraction pattern of TiO ₂	40
4.10 FT-IR spectra of TiO ₂	41
4.11 Effect of HA concentration on degradation by TiO ₂ photocatalyst (TiO ₂ dose 0.1 g/L, contact time 60min)	44

4.12 Effect of TiO ₂ dose on degradation of HA (HA conc. 5 mg/L, contact time 60 min)	45
4.13 Effect of contact time on degradation of HA by TiO ₂ photocatalyst, (a)HA conc. 5 mg/L, TiO ₂ dose 0.3 g/L, (b) HA conc. 14 mg/L, TiO ₂ dose 0.3 g/L	47
4.14 Effect of light intensity on degradation of HA by TiO ₂ photocatalyst, (a)HA conc. 5 mg/L, TiO ₂ dose 0.3 g/L, contact time from 30 – 180 min, (b) UV-C, HA conc. 14 mg/L, TiO ₂ dose 0.3 g/L, contact time from 30 – 180 min	48
4.15 The percentage of adsorption and photodegradation under UV-A and UV-C irradiation at different time	50
4.16 Catalyst reusability under UV-A and UV-C irradiation	51
4.17 Kinetics of HA degradation by TiO ₂ photocatalyst ($\ln(C_0/C_t)$ vs. t) at various initial HA concentration (TiO ₂ dose: 0.3 g/L), (a) UV-A; (b) UV-C	53
4.18 Kinetics of HA degradation by ZnO photocatalyst ($\ln(C_0/C_t)$ vs. t) at various initial HA concentration (ZnO dose: 0.3 g/L), (a) UV-A; (b) UV-C	56
4.19 Half-life of L-H kinetic of HA photocatalytic degradation	57

Chapter 1

Introduction

1.1 Background and Rationale

During recent years, the standards of water supply and sanitation in Indonesia is characterized as poor level considering the factors of access and service quality. The lack of access to clean water and sanitation is considered as a tough challenge, especially in rural areas. This is a major problem for the continuously increasing population, since the natural water is reducing level of drinking water quality. Among several water pollutants, Humic Acid (HA) causes serious water pollution problems around the world.

In the developing countries having peat forest around the territories, like in, Indonesia, problem is serious. In Indonesia, several sectors such as agriculture, peat forest fire and deforestation were the sources of peat land areas (Yustiawati et al., 2014). Peat land area plays an important role as the most significant contributor of HA formation, because HA is a Natural Organic Matter (NOM) which usually contain in peat soil as well as the forest. Water resources from some regions in Indonesia such as Kalimantan, Irian Jaya and Sumatra contain a lot of HA (Setyawati., 1994).

HA are natural polymers, formed from the microbial decomposition of animal and plant residues. HA can influence the performance of some pollutants considerably in natural environment. Some of such pollutants are trace metal speciation and toxicity, adsorption of hydrophobic pollutants. HA can act as a substrate for bacterial growth. It has the capability to prevent the bacterial degradation of contaminations in natural water. HA can act as an agent for heavy metals such as Pb, Mn and Fe making complex form. It is difficult to eliminate and transport the metals in the environment. The chemical structure of HA is complex and resist to degrade. Disinfection of water containing HA using chlorine as disinfectant can produce organochlorines which are toxic compounds as HAs react with chlorine and forms hazardous disinfection by-

products, e.g., trihalomethanes (THM), haloacetonitriles, haloacetic acids (HAAs) and haloketones.

Some conventional methods have been applied in order to remove HA from water, e.g. coagulation, flocculation, adsorption, and biofiltration (Zhang et al., 2005). Taking into account the disadvantage of these methods, the photocatalysis can be considered as an effective alternative solution for the elimination of HA in a water environment. Hepplewhite et al. (2004), reported that the concentration of HA is present in natural water sources in between 2 and 15 mg/l.

Recently, photocatalytic degradation processes involving Titanium Dioxide (TiO_2) have been applied as an alternative and showed a great potential for HA removal. TiO_2 particle when illuminated with wavelength ≤ 380 nm, produces excited-state electrons and hole pairs. The hole will interact with H_2O which produces powerful oxidizing agent, hydroxyl radicals and superoxides (Kerc et al., 2003). Moreover, Zinc Oxide (ZnO) is another alternative catalyst commonly used in photocatalytic degradation process. ZnO is used as an effective photocatalyst for organic pollutants degradation, due to its high photochemical reactivity, low cost and nontoxic. ZnO showed a good performance under UV irradiation which produces photon as energy in promoting generation of reactive oxygen species (ROS) (Ravichandrika et al., 2012).

Therefore, utilization of photocatalysis is a well-known processes to degrade the organic compound because of its environmental friendly, low-cost, and direct oxidation process can destruct complex molecules such as HA. The use of catalyst however creates a technical problem in retrieving the catalyst from the treated water. Hence, recovery and reusability is important during the photocatalytic process.

1.2 Objectives of study

In this study, batch experiments are conducted to investigate the degradation efficiency of the commercially available photocatalysts in the market in terms of percentage of HA degradation in drinking water treatment using TiO_2 and ZnO . The following objectives are identified for this study:

1. To examine the effects of initial HA concentration, catalyst dose, contact time, light wavelength and light intensity on the photocatalytic degradation process using TiO_2 and ZnO .
2. To investigate the kinetics of degradation of HA onto the catalyst surface by using the Langmuir-Hinshelwood model.
3. To discover the reusability of catalyst in optimum conditions.

1.3 Scope of study

In order to determine the efficiency of HA degradation by using photocatalysis process with two types of catalysts and to understand factors influencing the process, are taken into consideration. The scope of the study is as follows:

1. The HA solution with known concentration from 5 to 14 mg/L are prepared using HA sodium salt in the laboratory and investigated for photocatalytic degradation using TiO_2 and ZnO as catalyst.
2. The optimum condition required to achieve maximum degradation efficiency are determined by investigating the effect of HA concentration, catalyst dose, contact time, light wavelength and light intensity using synthetic water containing HA in batch experiment.
3. The commercial nanoparticle TiO_2 and ZnO as catalyst were obtained from Sigma Aldrich and stored at room temperature.

4. Both catalysts was characterized by several criteria i.e. XRD analysis, XRF analysis, BET analysis and FT-IR analysis.
5. Photocatalytic degradations were performed in a rectangular container, in which the dimensions were 20 x 30 x 20 cm batch photoreactor. This photoreactor were conducted in the seal condition, in which the containers were covered by aluminum foil.
6. The types of the lamp used are UV-A lamp and UV-C lamp. The wavelength range of the UV-A lamp is 315-400 nm, whereas in the UV-C lamp the range is 100-280 nm.
7. Pseudo-first order kinetics was used to understand the adsorption mechanisms and kinetics of HA degradation from the aqueous solution using photocatalysis in batch studies.

Chapter 2

Literature Review

For many decades, a number of research studies on degradation of Humic Acid (HA) have been investigated. Therefore, in accordance with the objectives of this study which has been proposed in the previous chapter is to review the literature related to the subject of further study. All information has to be investigated starting from the basic information about HA and the technology to degrade HA from water environment.

2.1 Humic Acids

2.1.1 Definition of Humic Substances

The main component of Natural Organic Matter (NOM) is defined as Humic Substances (HS) that are mixtures of amorphous polyfunctional, polydisperse, and heterogeneous polyelectrolytes whose conformations are primarily determined by environmental conditions. Humic Substances (HS) are major components of NOM not only in soil and water, but also other geological organic deposits like peats, sediments of lakes, brown coals and shales. HS are the reason for the characteristic brown color of decaying plant debris. Moreover, it gives the brown or black color in surface soils as well.

Humic substances are vital part of soil that affect physical and chemical properties and enhance soil fertility. In aqueous systems, for example in rivers, about 50% of the dissolved organic materials are HS that affect pH and alkalinity. The formation of disinfection by-products during water treatment can be affected to biological productivity in aquatic ecosystems (IHSS, 2013).

2.1.2 Classification of Humic Substances

In terms of the geological perspective, HS are chemical intermediates between plants and fossils. The chemical composition of soils, sludge and sediments can continuously change via the alteration and degradation of organic matter. Humification is a continuous historical process, and soil humus is a dynamic system of both chemically active and passive components (Gonzalez et al., 2003). Based on Figure 2.1, all the HS can be divided into components according to their solubility in different media. Humin represents the insoluble residue. HA are insoluble at low pH, and they are precipitated by adding strong acid. The types of HS differentiated by differences in solubility is indicated in the Table 2.1 below.

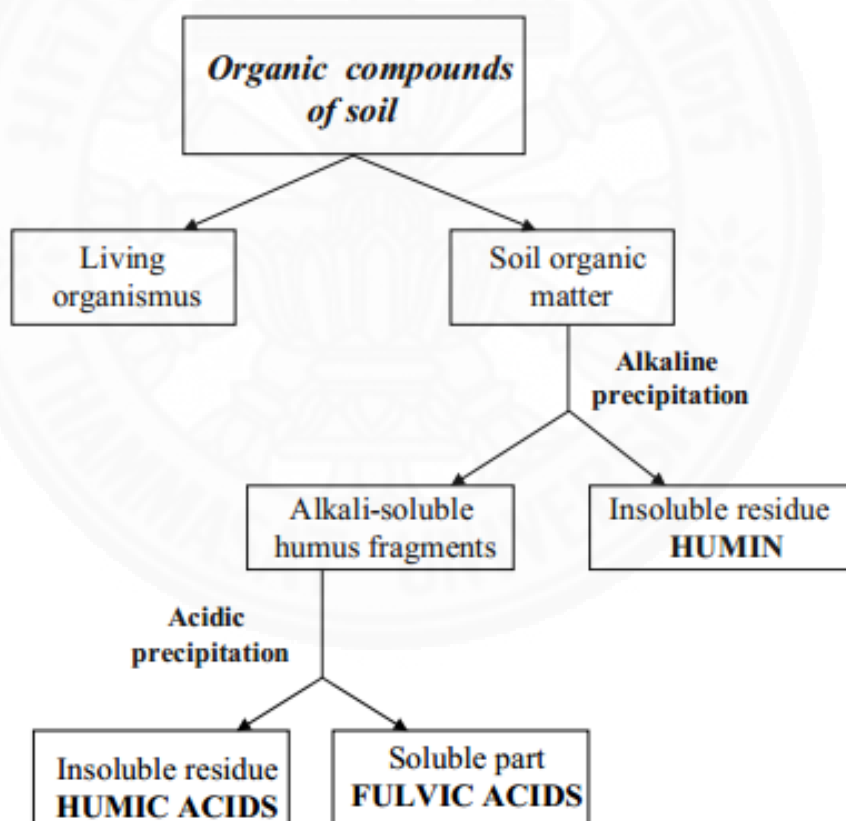


Figure 2.1 Schematic representation of humic substances in dependence of their solubility

Table 2.1 Major types of Humic Substances Characterized by Differences in Solubility

Type of Humic Matter	Alkali	Acid	Water
Fulvic Acid	Soluble	Soluble	Soluble
Humic Acid	Soluble	Insoluble	Insoluble
Humin	Insoluble	Insoluble	Insoluble

Source: (Kim H., 2005)

Humic substances are mostly chemically reactive yet recalcitrant to biodegradation. The actual properties and structure of a specific HS sample depends on the source of water or soil and the provided conditions of extraction. Figure 2.2 shows the differences of chemical properties between HA and FA.

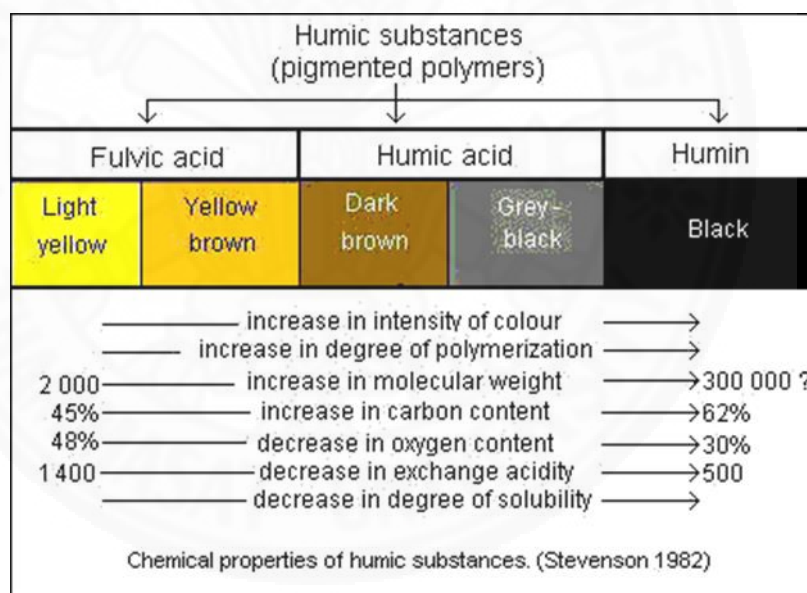


Figure 2.2 Properties of Humic Substances

2.1.3 Definition of Humic Acid

It is the key constituent of dissolved organic matter. HA can be deposited in natural water due to the decomposition of living bodies, plants and other biological activities of microorganisms in system of the nature. HA in water may cause unacceptable taste and color and also act as a catalyst for bacterial growth in water

based systems. Moreover, HA molecules have the ability to bond with aqueous heavy metals, pesticides, and herbicides. Moreover, HA can be affected to chlorine disinfectants as well. Thus, the need to remove HA is vitally important especially in terms of drinking water quality (Peng et al., 2005).

2.1.4 Source of Humic Acid

HA contain aromatic blocks is characterized by a broad molecular weight distribution and high chemical heterogeneity. Table 2.2 shows the distribution of organic compound in natural water. Humic acid can act as substrates for bacterial growth, inhibit the bacterial degradation of impurities in natural water, form a complex with heavy metals such as Fe, Pb, Mn making to be harder to remove them and transport the metals in the environment (Zhao et al., 2013).

Table 2.2 The Distribution of Organic Compounds in Natural Water

Class	Subclass	% DOC
Humic Substances	Fulvic Acid	40
	Humic Acid	10
Hydrophilic Acids		30
Specific Organic Compounds	Carbohydrates	9
	Carboxylic Acids	7
	Amino Acids	3
	Hydrocarbons	1

2.1.5 Chemical Structure of Humic Acid

The molecule of HA is one fragment of huge molecule. The fragments are connected to each other in long chains and total weight of molecules, naturally depending on the chain length, is in the range from 35 000 to 80 000 Daltons. It shows in Figure 2.3 below. It is observed that chemical structure of HA is mostly consisted of quinoid, carboxyl, and hydroxyl, phenolic groups.

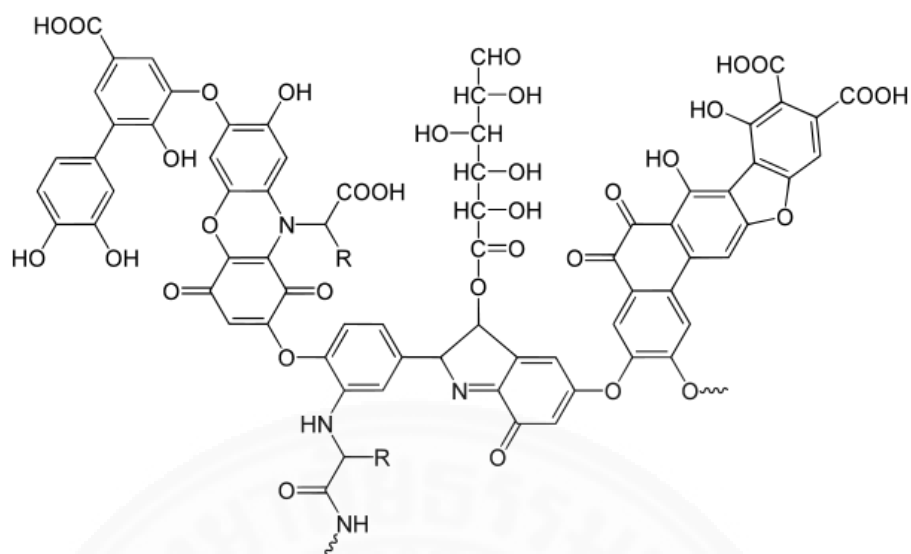


Figure 2.3 Chemical Structure of Humic Acid

2.1.6 Impact of Humic Acid Pollution on Organism and Environment

Different effects of HS in natural environment can be expected regarding to its chemical constitution. Until recently, mainly indirect effects of HS in the ecosystems have been discussed. Indirect effects of HA on organisms include in particular both heavy metals and nutrients control and modulating of toxicity of pesticides and other xenobiotics. However, in the larger sense, all the issues mentioned in Table 2.3 (except the last item) represent possible indirect effects of HS on living organisms.

Table 2.3 Environmental issues involving HS

Issue	Role of humic substances
Carbon cycling	Major C pool, transformations, transport and accumulation
Light penetration into waters	Absorption and attenuation of light by humic chromophores
Soil warming	Absorption of solar radiation by soil humic matter
Soil and water acidification	Binding of protons, aluminium and base cations in soils and waters
Nutrient source	Reservoir of carbon, nitrogen, phosphorus, sulphur and chlorine
Nutrient control	Binding of iron and phosphate
Microbial metabolism	Substrate for microbes
Weathering	Enhancement of mineral dissolution rates
Soil formation (podzolisation)	Translocation of dissolved humic substances and associated metals (Al, Fe)
Properties of fine sediments	Adsorption at surfaces and alteration of colloidal properties
Soil structure	Aggregating effect on soil mineral solids
Photochemistry	Mediation of light-driven reactions
Heavy metals	Binding, transport, influence on bioavailability, redox reactions
Pesticides, xenobiotics	Binding, transport, influence on bioavailability
Radioactive waste disposal	Binding and transport of radionuclide ions in groundwaters
Ecosystem buffering	Control of proton and metal ion concentrations, persistence
Direct biological effect	Uptake and direct interaction with living organisms

Source: (Tipping, 2002)

2.2 Measurement of Humic Acid in a Water Environment

The HAs content of raw water is an important analytical parameter in water treatment facilities since they have been associated with the formation of carcinogenic disinfection by-products (e.g. trihalomethanes) upon chlorination of drinking water (Wang, 2001). HA adversely affect the quality of drinking water since they impart colour and serve as precursors for the formation of chlorinated compounds. In a

natural water system, HA is present in concentrations ranging from 0.1 to 200 mg /l (Kinniburgh et al., 1999) and in drinking water at concentration levels of between 2 and 15 mg/l (Hepplewhite et al., 2004). They also have complexing properties that include association with toxic elements and micro-pollutants (De Wuilloud et al., 2003).

2.3 Methods for Humic Acid Treatment

HA commonly reported to carry many negative effects in drinking water, including undesirable color and taste, absorption and concentration of organic pollutants, and biochemical decomposition. Moreover, when water is treated with chlorine for sterilization, HA could react with chlorine by a combination of substitution and oxidation mechanisms forming potentially carcinogenic organic compound. This has been a problem in past drinking water treatment. Increased concern is focused on the potential toxicity of HA and its precursors. Hence, the degradation techniques of HA need to be established.

In common water treatment processes, the removal of HA has been accomplished by physical separation, such as adsorption of activity carbon, precipitation and flocculation, ion exchange and transfer of pollutants from one phase to another or concentrating them in one phase, without actually eliminating them, which is the main disadvantage associated with these techniques. Degradation methods such as the fenton process, ozonation, and electrochemical, photochemical and photocatalysis technologies have been developed to decompose pollutants. The comparison of technologies to remove HA is mentioned in Table 2.4 below.

Table 2.4 The Comparison of Technologies to Remove Humic Acid

No.	HA Removal Technology	Removal Efficiency	Remarks	Reference
1.	Ultrafiltration Membranes	“Removal efficiency of UF membrane of 85-90% at humic acid concentration over 7.5 mg/L, while MF membrane are very efficient only if used in tubular configuration, reaching organic matter removal of 90%.”	<ul style="list-style-type: none"> - Effective to remove particles higher than their size. - Provide maximum quality using a very low energy - Short membrane life-time - Fouling 	(Marina P. et al., 2013)
2.	Coagulation	“The initial HA concentration increased from 500 to 750 mg/L, the oxidation removal increased from 74.9 to 77.3%; whereas only 1.6% of oxidation removal increment was achieved as the initial HA concentration enhanced from 750 to 1000 mg/L.”	<ul style="list-style-type: none"> - High maintenance and operation costs - Minimizing the residues amount until 0% (Fenton system) - Simple technique to follow 	(Wu Y et al., 2011)
3.	Ion Exchange	“The reversibility was expressed as percent recovery of color, 27-69% for phenolic weak-base resins but only 0.7-9.5% for polystyrenic strong-base resins.”	<ul style="list-style-type: none"> - Effectively remove ions - Not efficient in removing most organics or microorganisms. - High maintenance/operation costs - Complicated procedure involved in the treatment 	(Abraham and Breslin., 2009)

No.	HA Removal Technology	Removal Efficiency	Remarks	Reference
4.	Adsorption	“Humic acid removal was relatively fast with more than 50 % of peat water removed in ≤ 15 min. The maximum humic acid removal of about 94.56 % was observed at the dosage of 5 g.”	<ul style="list-style-type: none"> - Easy to find the adsorbent in environment - Comparatively cheap - Effectively used as an adsorbent for HA removal in a peat water 	(Bhaumik et al., 2012)
5.	Photocatalysis	“Received 88% of TOC removal with optimum TiO ₂ loading of 1.0 g/l after 6 h of irradiation.”	<ul style="list-style-type: none"> - Can be an alternative to remove the organic pollutants - Applicable in the real application of water treatment 	(Rajabi H et al., 2013)

2.4 Photocatalyst Degradation of Humic Acid

2.4.1 Photocatalyst

Catalysis is the process which involves in participating the substance in modifying the rate of a chemical transformation of the reactants without being altered or consumed in the end. This substance is known as the catalyst which increases the rate of a reaction by reducing the activation energy. Titanium dioxide (TiO₂) and zinc oxide (ZnO) are well-known photocatalysts used in photodegradation of organic compounds due to their high photoactivity, low cost and non-toxic. To enhance the photodegradation activity, a semiconductor photocatalyst often combines with another semiconductor so as to build a heterojunction at the interface (Sajjad, 2009). On the basis of the same idea, mixed-phase anatase, rutile TiO₂ nanoparticles has also been used to photodegrade HA (Yigit et al., 2009).

2.4.2 Photocatalysis

Photocatalysis is a reaction which uses light irradiation as a source of energy to activate a substance which can be modified the rate of a chemical reaction without being involved itself. Degradation of HA irradiated by UV light in the presence of catalyst were faster than irradiated in the absence of catalyst. With the same time of irradiation, a significant reduction of HA by about 80% was observed. This case could be explained that species reactive in the solution are produced from HA itself which act as sensitizer and also from catalyst (Andayani, 2011).

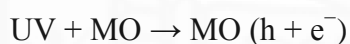
TiO₂ and ZnO have been universally used as a photocatalytic with applications in many fields such as environmental purification and decomposition of carbonic acid gases and solar cell, especially in the decomposition of recalcitrant organic pollutants. It has been demonstrated that TiO₂ and ZnO photocatalysis are the suitable advanced oxidation processes (AOPs) techniques for the decomposition of refractory HA because of its excellent photostability, relatively low cost, nontoxicity, and its ability to photooxidatively destroy most refractory pollutants (Bekbolet, 2007). Jarek et al. (2002) showed that the photocatalysis process can break long organic molecules into

smaller biodegradable compounds and can make their biological treatment eligible. It may at the end reduce the cost of process.

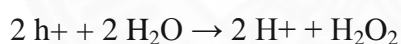
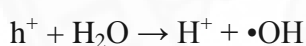
2.4.3 Mechanism of Photocatalysis

The heterogeneous photocatalysts are transition metal oxides and semiconductors. When a photon with higher energy level than the semiconductor band gap. The electron is jumped from the valence band to the conduction band. Due to the generation of positive holes and electrons, the reactions of oxidation-reduction occurred at the surface of semiconductors. The positive holes will react with the moisture on the surface and produce a hydroxyl radical during the oxidation reaction, as shown in Figure 2.4 below.

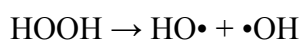
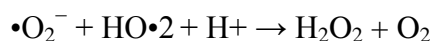
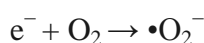
Oxidative reactions due to photocatalytic effect:



Here MO stands for metal oxide ---



The reductive reaction due to photocatalytic effect:



Ultimately, the hydroxyl radicals are generated in both the reactions. These hydroxyl radicals are very oxidative in nature and non selective with redox potential of ($E_0 = +3.06 \text{ V}$) (Daneshvar et al., 2004).

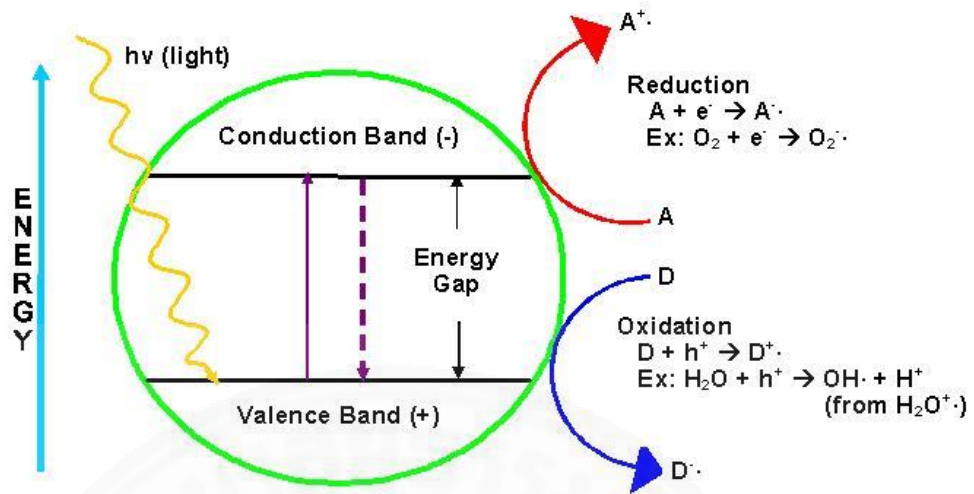


Figure 2.4 Mechanism of photocatalytic process and the reactions that occur at the surface

2.4.4 Parameters Affecting The Photocatalytic Degradation

Some of the operation parameters are vital which are affected subsequent to the integrating of the semiconductor catalyst with a photoreactor, the oxidation rates and efficiency of the photocatalytic system. These parameters dominate the kinetics of photomineralization and photo-disinfection, such as catalyst dose, contaminant concentration, light wavelength and light intensity.

Catalyst loading interprets the amount of catalyst dose in the system. Concentration of catalyst in the photocatalytic water treatment system clearly affects the overall photocatalysis reaction rate in a true heterogeneous catalytic regime, in which the amount of catalyst is directly proportional to that of the overall photocatalytic reaction rate (Gaya and Abdullah, 2008).

A difference in the initial concentration of the water pollutants will result in changed irradiation time essential to achieve complete mineralization or disinfection, given that the operating conditions are similar (Saqib and Muneer, 2003).

For the case of UV types, the corresponding electromagnetic spectrum can be characterized as UV-A, UV-B and UV-C. This classification is based on the difference of emitting wavelength. The UV-A contains light wavelength range of 315 to 400 nm (3.10-3.94 eV). On the other hand, UV-B contains a wavelength range of 280-315 nm (3.94-4.43 eV). The germicidal UV-C wavelength range is reported as 100 to 280 nm (4.43-12.4 eV) (Rinco'n and Pulgarin, 2005).

The photonic nature of the photocatalysis reaction is clearly affected by the type of light intensity used since it provides the specific photons for the catalyst to produce hydroxyl radicals. If a high photocatalytic reaction rate to be achieved, mostly in the case of treatment of water, a comparatively high light intensity is essential to sufficiently provide each catalyst surface active sites with enough photons energy necessary.

2.4.5 The kinetics of photocatalysis

Chemical kinetics describe about the time dependent analysis of the quantity of a substance which is subjected to a chemical reaction. Many photocatalytic processes are been studied using different kinetic models mainly from pseudo-first order and second order models. The integral of these differential equations gives an idea about the decay rate or amount of the compound, which is undergoing photocatalysis.

Since single reactant is concerned in this study, pseudo-first order kinetic model is used to find the relationship the adsorption mechanisms and kinetics of HA degradation. The description of the kinetic model is mentioned in detail in Chapter 3.

Chapter 3

Methodology

This study focuses on batch experiments to investigate the technical feasibility of using photocatalysis for Humic Acid (HA) degradation under UV irradiation. Two types of catalyst were used such as Titanium dioxide (TiO_2) and Zinc Oxide (ZnO). For HA degradation from aqueous solution, the batch studies were carried to find out the optimum conditions of pertinent factors, which include the light wavelength, light intensity, HA concentration, TiO_2 dose and contact time.

3.1 Materials and Methods

3.1.1 Preparation of synthetic HA solution

HA stock solutions are prepared by using Sigma Aldrich laboratory-grade humic acid-sodium salt solution. HA concentration of 5, 8, 11 and 14 mg/L were prepared from the stock solution of 1000 ppm and diluted by using serial dilution as usually HA concentration appeared in drinking water from 2 – 15 mg/L (Hepplewhite et al., 2004). Before using, HA sodium salt was dried in an oven for 4 hours at 105°C . In order to make standard calibration curve of HA, weigh out the dried HA about 0.1075 g and dilute to 100 ml for 1000 ppm. The standard curve was made using 5, 10, 15, 20 and 25 mg/L of HA.

3.1.2 Titanium dioxide (TiO_2) as catalyst

Titanium Dioxide nanoparticles with anatase and rutile phases manufactured by Sigma Aldrich, an average particle size of 21 nm, $\geq 99.5\%$ purity based on trace metals analysis, was used as catalyst.

3.1.3 Zinc oxide (ZnO) as catalyst

Commercially available Zinc Oxide nanoparticles with a size of 6-12 nm, crystal structure hexagonal, 99.8% purity, was used. Because ZnO nanoparticles are more difficult to disperse in organic solvent, ultrasonication for 5-10 min is required for dispersion in solution.

3.2 Experimental Equipment and Procedure

3.2.1 Experimental Equipment

Table 3.1 Parameter and Equipment used

Parameter	Items	Model
Catalyst dose, HA concentration, Contact time and Light intensity	Ultrasonic	Ultrasonic Cleaner with Heater VGT-1860QTD
	Spectrophotometer	Thermo Scientific Genesys 10S UV-Vis
	UV Meter	LT lutron YK-37UVSD
	Centrifuge	DiGi Cen 21-Ortoaires Max. 5000 rpm
	Magnetic Stirrer	SCI-LOGEX M57-H550-S
	Orbital Shaker	N-Biotek, NB-101 M RPM: 30-300 rpm
	Oven	Binder

3.2.2 Experimental Procedure

The experiment is conducted in batch system. Batch studies deal with the study of TiO₂ and ZnO photocatalytic degradation of HA from drinking water. Generally, the overview of experiment can be illustrated by a flowchart in Figure 3.1.

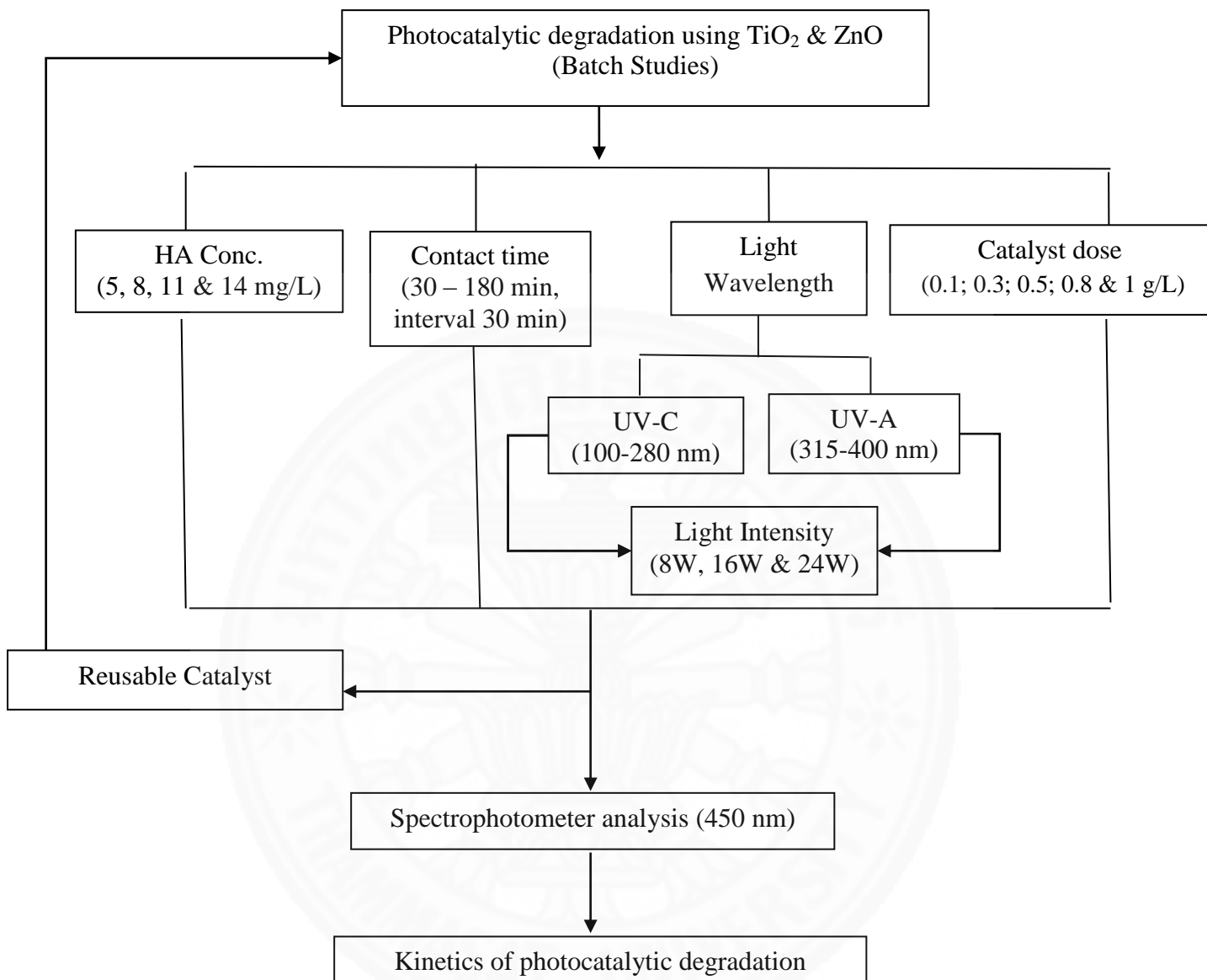


Figure 3.1 Overview of the batch photocatalytic degradation of HA

3.2.2.1 Photocatalytic Reactor

Photocatalytic degradations were performed in a rectangular container, the dimensions of the batch photoreactor are 20 x 30 x 20 cm. Photoreactor was covered by aluminum foil. Two reactors are for each UV-A and UV-C lamp, were used. One lamp was installed at the top of the reactor, and two of lamps were installed on each side of the container. The wavelength range of the UV-A lamp is 315-400 nm,

whereas in the UV-C lamp the range is 100-280 nm. Effect of light intensity was measured on the liquid surface by varying the number of 8W UV-A lamps i.e. 0.131 mw/cm^2 , 0.167 mw/cm^2 and 0.236 mw/cm^2 , respectively. For the case of UV-C, the light intensities were 0.196 mw/cm^2 , 0.233 mw/cm^2 and 0.284 mw/cm^2 , respectively. Photocatalytic experiment was done in a Pyrex beaker placed on the top of magnetic stirrer containing 100 ml of HA solution at the concentration of 5, 8, 11 and 14 mg/L. The catalyst dose was varied from 0.1 – 1 g/L. The suspensions were irradiated for various contact time ranging from 30 – 180 min in interval of 30 min. After irradiation, the suspensions were filtered using 0.45 μm syringe filters. All experiments were performed at room temperature ($25 \pm 3^\circ\text{C}$) and at neutral pH conditions. The setup of the equipment is indicated in the Figure 3.2 below.

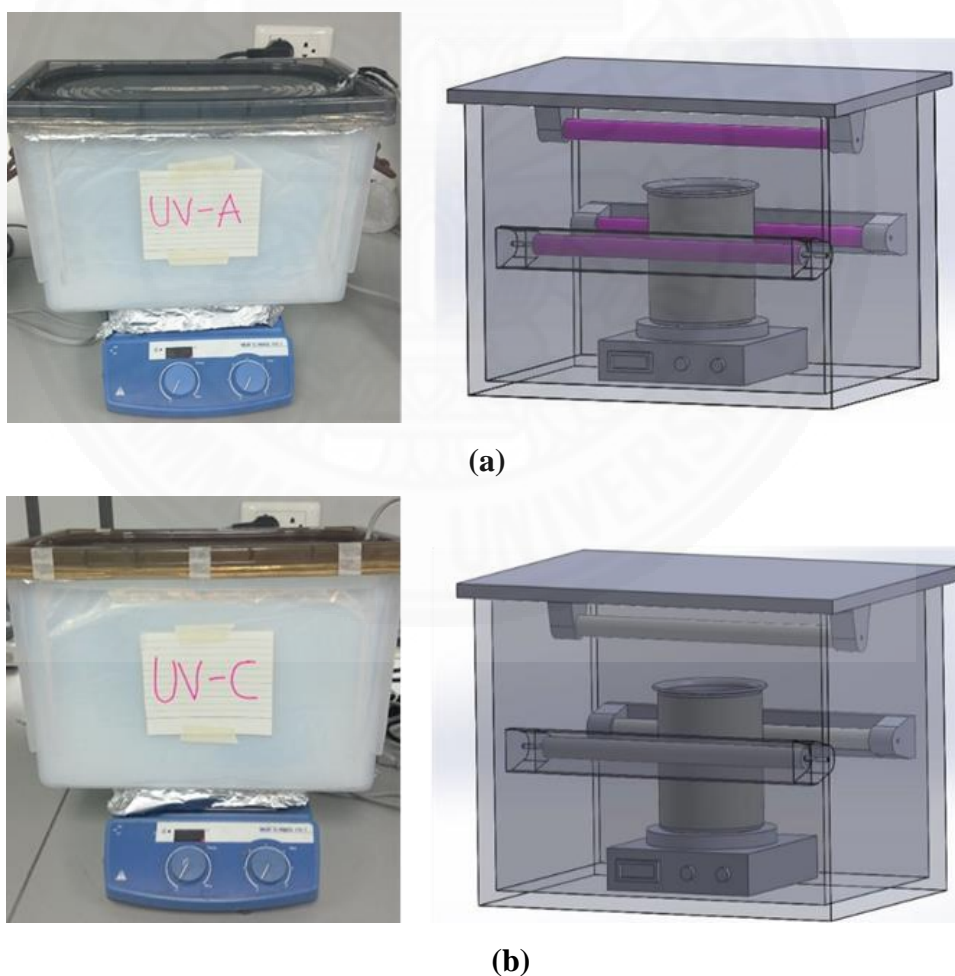


Figure 3.2 Schematic of the photocatalytic reactor
(a) UV-A; (b) UV-C

3.2.2.2 HA Analysis Method

HA concentrations were analyzed by using UV-visible spectrophotometer Thermo Scientific, Genesys at 276 nm wavelength with 1 cm quartz cell. Standard calibration curve relating absorbance and concentration were developed. The method detection limits for HA is 4.62 mg/L and quantitation limits for HA is 14.7 mg/L, respectively (IHSS, 2015).

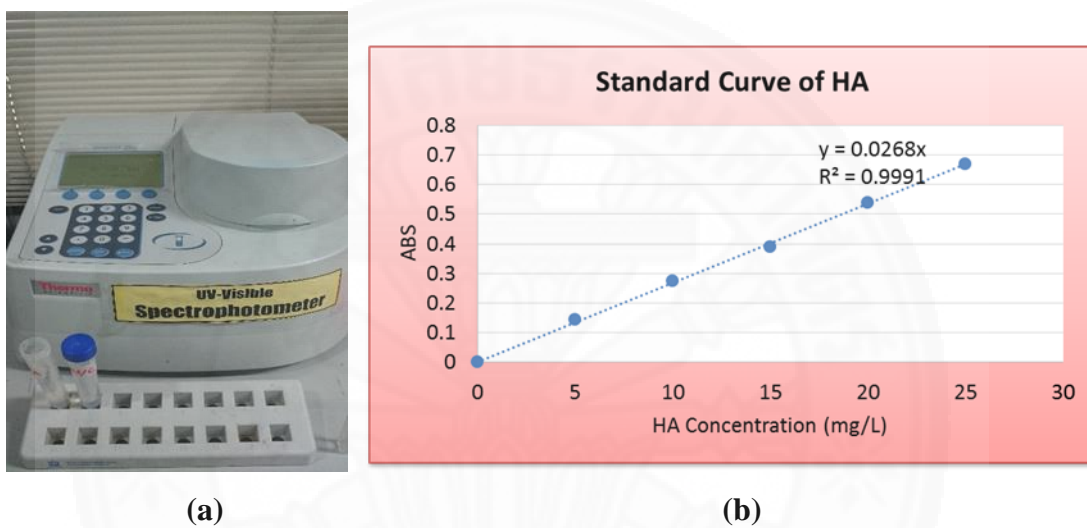


Figure 3.3 HA Analysis Methods
(a) Spectrophotometer
(b) Standard Curve of HA

3.3 Batch Experiments

The photocatalytic degradation by batch technique were conducted at room temperature from 25-27°C. The pertinent factors as mentioned above were varied to determine the optimum condition for the maximum degradation of HA in the aqueous solution. All the experiments were conducted in duplicate.

3.3.1 Effect of Catalyst dose

Catalyst dose is the important affects to the reaction rate of photocatalytic process. In this experiment, TiO₂ and ZnO concentrations as catalyst employed are 0.1, 0.3, 0.5, 0.8 and 1 g/L. The optimum condition for using catalyst was conducted at condition with HA concentration of 5 mg/L in 60 min.

3.3.2 Effect of HA Concentration

After finding the optimum dose of catalyst, experiment were conducted to determine the efficiency of photocatalysis to degrade HA in the aqueous solution. For this HA concentration were varied from 5, 8, 11 and 14 mg/L. Before using HA, it was dried at 105°C for 4 hours, after that stock solution was diluted (100 mg/L).

3.3.3 Effect of Contact Time

The degradation of HA is also studied as a role of contact time using the optimum conditions of catalyst dose, HA concentration, light wavelength and light intensity. The rate at which degradation takes place is an important factor in a photocatalysis system. To study the effect of contact time, experiments were conducted by varying the contact time from 30 to 180 min at an interval of 30 min.

3.3.4 Effect of Light Wavelength

Depending on the photocatalyst types, light sources with different wavelength will have a significant effect on the photocatalytic reaction rate in photo degradation. In this experiment commercial nanoparticle TiO₂ and ZnO, were used. Two types of UV lamp were used, UV-A lamp and UV-C lamp. The wavelength range of the UV-A lamp is 315-400 nm (3.10 - 3.94 eV), whereas in the UV-C lamp is in the range of 100-280 nm (4.43 – 12.4 eV). Two different reactors were used for UV-A lamp and UV-C lamp.

3.3.5 Effect of Light Intensity

The term intensity was used to describe the rate at which light spreads over a surface of a given area some distance from a source. Effect of light intensity was investigated by varying the number of lamps from 1, 2 and 3. Each lamp has a power of 8 watt. Therefore, the intensity for UV-A lamps was 0.131 mw/cm², 0.167 mw/cm² and 0.236 mw/cm², respectively. For UV-C lamps, the light intensity was 0.196 mw/cm², 0.233 mw/cm² and 0.284 mw/cm², when using 1, 2 and 3 lamps, respectively.

3.3.6 Catalyst reusability

In this experiment, after the reaction is completed, catalyst was separated from the reaction mixture by using centrifuge for 20 min at a speed of 5000 rpm. The reusability of the catalyst was assessed after drying the catalyst at 60°C for at least 12 h.

3.3.7 The kinetics of photocatalytic degradation

The photocatalytic rate of organic contaminant over irradiated catalyst fitted to pseudo first order kinetics. A single-site pseudo first order model is proposed to calculate photocatalytic degradation rates, since only one contaminant is used in this experiment.

$$r = -\frac{dC_t}{d\tau} = \frac{kKC_t}{1+KC_t} \quad (3.1)$$

Where r is the reaction rate (ppm min⁻¹), t is the irradiation time (min), k is the apparent kinetic constant (ppm min⁻¹), K is the adsorption equilibrium constant (ppm min⁻¹), C_t is the contaminant concentration at time t (ppm). If KC_t is much smaller than 1, the reaction is a first-order reaction containing a constant reaction rate coefficient. Eq.(3.1) can be modified as Eq.(3.2). First-order oxidation kinetics can be seen when C₀ is insignificant.

$$r = -\frac{dC_t}{d\tau} = K'C_t \quad (3.2)$$

Where K' is the apparent first-order reaction coefficient (min^{-1}). The integrated arrangement of Eq.(3.2) is shown from Eq.(3.3).

$$C_{\tau} = C_0 e^{-K' \tau} \quad (3.3)$$

Logarithmic function can be used to Eq.(3.3) in order to linearly interpret the relationship as Eq.(3.4).

$$\ln C_0 - \ln C_{\tau} = K' \tau \quad (3.4)$$

Eq.(3.4) indicates that $\ln C_t$ is strong linearly related to t during the photocatalytic process providing with KC_t far less than 1 and that the slope of the fitted straight line equals to the apparent first-order reaction coefficient K' . Half-life ($t_{1/2}$) of photocatalysis can be computed by Eq.(3.5) which illustrates the stage where the contaminant concentration is decreased to 50% of its initial amount.

$$t_{1/2} = \frac{0.693}{k} \quad (3.5)$$

$t_{1/2}$ can be used to compute the photocatalytic rates at dissimilar K' and initial concentrations.

3.3.8 Characterization of catalyst

3.3.8.1 XRD Analysis

The X-Ray Diffraction (XRD) analysis was performed using a X-ray diffractometer, PANalytical PW3040/60 X'Pert PRO apparatus. The voltage and anode current used are 40 kV and 30 mA, respectively. The step angle is 0.02° , the count time every 0.5 second, D-, R- and S-slits 1° , $1/2^\circ$ and $1/4^\circ$, respectively, the $\text{CuK}\alpha = 0.15406 \text{ nm}$. XRD analysis was conducted at The National Metal and Materials Technology Center (MTEC), Science Park, Pathumthani, Thailand.

3.3.8.2 BET Analysis

The measurement of the surface area by Brunauer, Emmett and Teller (BET) methodology was applied using the surface analyzer by gas adsorption technique (Nitrogen gas only), autosorb from Quantachrome Instrument, USA. The information extracted from this equipment allows the evaluation of the precise value of the total surface area in m^2/g . BET analysis was conducted at The Nanotechnology (NANOTEC), Science Park, Pathum Thani.

3.3.8.3 FT-IR Analysis

The composition quality of the material was characterized by Fourier transform infrared (Thermo Nicolet 6700 FT-IR spectrophotometer) spectroscopy in the mid-infrared range ($400\text{--}4000\text{ cm}^{-1}$). The graph was plotted between % transmittance and wavenumber (cm^{-1}). FT-IR analysis was conducted at The National Metal and Materials Technology Center (MTEC), Science Park, Pathum Thani.

3.3.8.4 XRF Analysis

The elements inside of catalyst was measured by X-Ray Fluorescence spectrometer, Bruker model S8 Tiger in the wavelength dispersive method. XRF was conducted at Scientific and Technological Research Equipment Centre, Chulalongkorn University.

3.3.8.5 TOC Analysis

The Total Organic Carbon was performed by the SHIMADZU TOC-LCPH/CPN, pc-controlled model of TOC analyzers. It adopts the 680°C combustion catalytic oxidation method for liquid sample and the TOC ssm-5000a using the swab method for solid sample.

Chapter 4

Results and Discussions

4.1 HA Degradation by ZnO Photocatalyst

4.1.1 Characteristic of ZnO as a catalyst

4.1.1.1 XRD Analysis

In this study, the catalyst characterization analysis was performed by X-ray diffractometer. The XRD pattern of ZnO referring to Fig. 4.1 clearly indicated that the particles were pure and crystalline in nature. The peaks (2θ value) observed at 31.7° , 34.3° , 36.3° , 47.6° and 56.7° were assigned to (100), (002), (101), (102) and (110). This proves the fact that characteristic peaks represent the ZnO with hexagonal phase. Similar, X-ray diffraction pattern were reported by previous researchers (Chena et al., 2011; Yong et al., 2012).

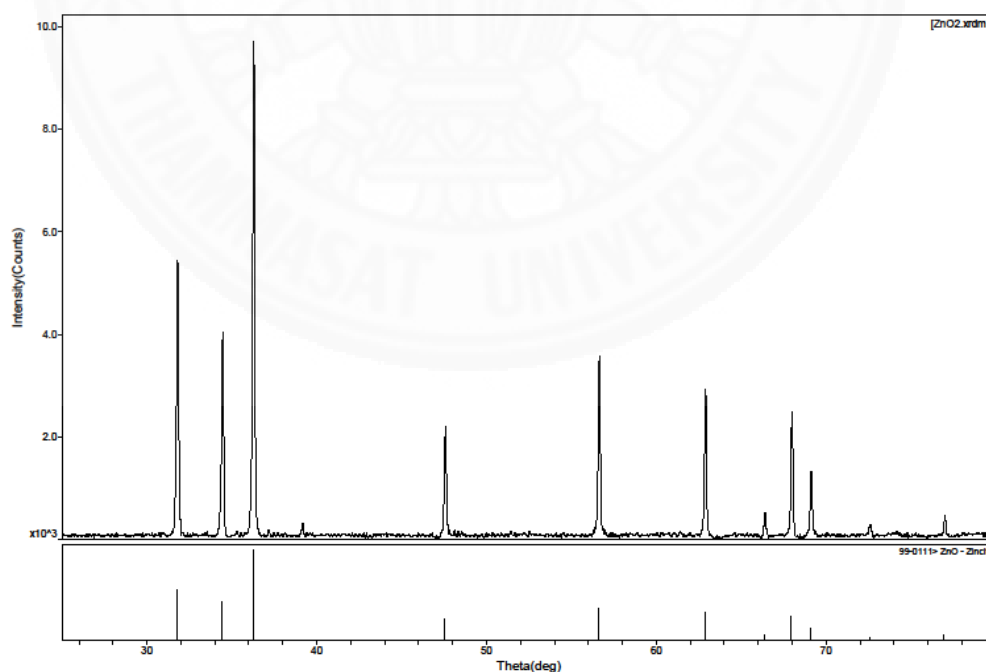


Figure 4.1 X-ray diffraction pattern of ZnO

4.1.1.2 FT-IR Analysis

Figure 4.2 shows the FT-IR spectra of the initial ZnO and after photocatalytic treatment under UV-A and UV-C, respectively. FT-IR spectra of the ZnO nanoparticles showed a peak at 3442.64 cm^{-1} corresponding to the O-H stretching of water adsorbed on the ZnO surface. Peak at 2360.53 cm^{-1} corresponds to C-H stretching vibration and 1365 cm^{-1} corresponds to C=O asymmetric C=O stretching. Furthermore, a peak at 1630.49 cm^{-1} corresponds to H-O-H bending. Metal oxides generally give absorption bands in fingerprint region below 1000 cm^{-1} arising from inter-atomic vibrations. For examples, those observed around 436.66 cm^{-1} as Zn-O stretching and deformation (Fryxell et al., 2007).

FT-IR spectra under UV-A and UV-C shows similar pattern as seen in Figure 4.2. Compared to the initial, the peak at 2360.53 cm^{-1} which corresponds to C=O stretching of CO_2 disappeared and a new absorption peak appeared at 879.11 cm^{-1} and 912.90 cm^{-1} for UV-A and UV-C, respectively, due to =C-H bending vibration as the byproduct of HA degradation. The peak of O-H stretching vibration shows the interaction between the molecules, which effected the sliding of peak at 3442.64 cm^{-1} of initial to 3438 cm^{-1} and 3431 cm^{-1} for UV-A and UV-C, respectively. The molecules of H_2O released as a result of adsorption of HA onto the ZnO through O-H bond. Similar shift phenomenon is appeared for H-O-H bending vibration. The shift of peak occurred at 1630.49 cm^{-1} to 1626 cm^{-1} and 1623 cm^{-1} for UV-A and UV-C, respectively, shows that the energy of H-O-H bending vibration decrease.

Gierlach et al and Amir et al (2004), reported the FT-IR spectra of the HA, the assignments of the main recorded bands are: the HA exhibit a strong absorption band at $3600\text{--}3200\text{ cm}^{-1}$ that is due to the presence of H-bonds between OH groups, absorption at $2920\text{--}2860\text{ cm}^{-1}$ coming from stretching vibrations of $-\text{CH}_3$ and $-\text{CH}_2$, absorption at 1720 cm^{-1} and $1230\text{ to }1200\text{ cm}^{-1}$ originating from carboxyl groups, absorption originating from amide groups at 1660 cm^{-1} , conjugated C=C bonds at 1610 cm^{-1} , and at $1100\text{--}1000\text{ cm}^{-1}$ originating from aliphatic OH present predominantly in carbohydrates. Several peaks were disappeared indicating the

reduction of functional groups of HA. As the HA functional groups disappear, another by product is assumed be formed on the catalyst surfaces. Hence, a new peak appeared as mentioned previously.

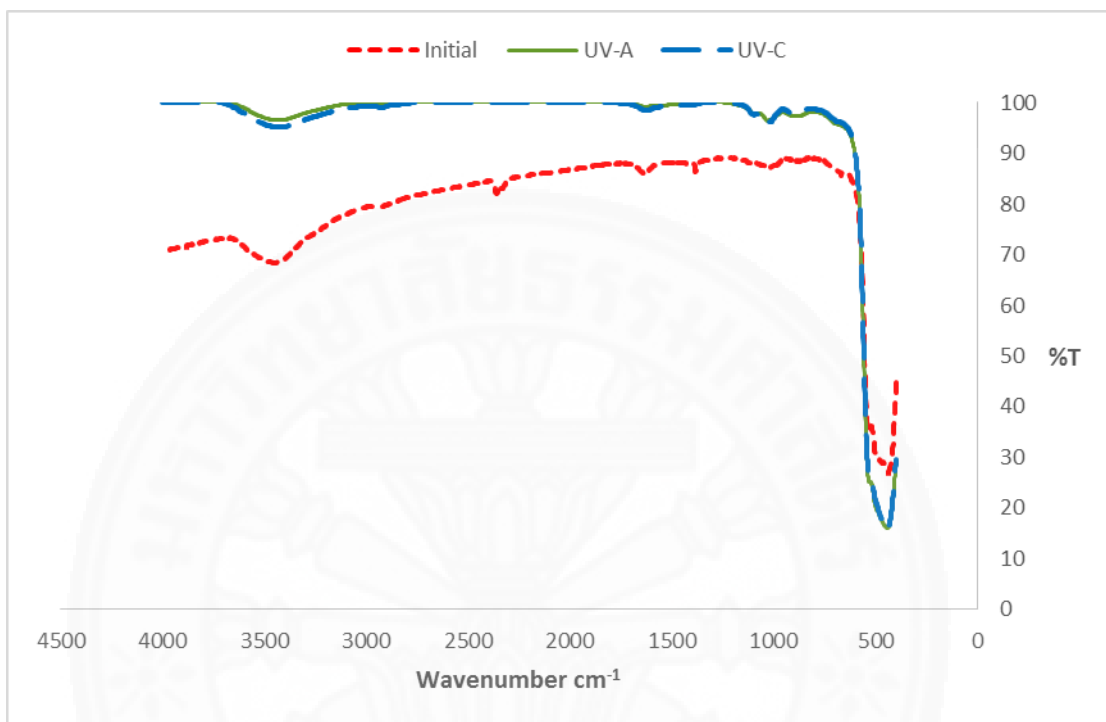


Figure 4.2 FT-IR spectra of ZnO

4.1.1.3 BET Analysis

The specific surface area is one of key factor to determine the photocatalytic activity of the photocatalyst since the redox reactions take place on the surface of the photocatalyst. Therefore, the BET analysis of the surface area was required to check the morphology of photocatalysts. Table 4.1 indicates the properties of ZnO based on BET analysis before and after photocatalytic process. After the photocatalytic process, the agglomeration of the catalyst results in lower specific surface area. It is a well-known fact that the cause for this agglomeration is due to hydrogen bonding. However, insignificant reductions were observed on the surface area of catalysts after photocatalytic process. This implies that the catalyst can be reused further up to several cycles.

Table 4.1 Properties of ZnO based on BET analysis

Parameter	Specific surface area (m²/g)	Total pore volume (cm³/g)	Pore diameter (nm)
ZnO (Initial)	50	0.025	2.089
ZnO (UV-A)	48.71	0.024	2.053
ZnO (UV-C)	46.05	0.023	2.071

4.1.1.4 XRF Analysis

Table 4.2 indicates the ZnO elements based on XRF analysis before and after photocatalytic process. The initial XRF analysis of ZnO indicated 100% purity. After photocatalytic treatment, it was found that the amount of ZnO decreased. Moreover, several elements were attached on the ZnO surface. The elements of SiO₂, Fe₂O₃, TiO₂ were attached on the ZnO surface as a results of compositions of HA. The HA composition indicated in Appendix. 1 shows that the HA contains several inorganic elements i.e iron, silicon and titanium.

Table 4.2 ZnO elements based on XRF analysis

Element	ZnO	SiO₂	Fe₂O₃	TiO₂
	%	%	%	PPM
ZnO (Initial)	100	–	–	–
ZnO (UV-C)	99.2	0.558	0.149	327

4.1.2 Pertinent factors of HA degradation

4.1.2.1 Effect of HA concentration

The effect of HA concentration of was carried out at 0.1 g/L ZnO dose, for 60 min. HA concentrations was varied from 5 to 14 mg/L. From Fig. 4, it can be seen that with an increment of the initial concentration of HA can reduce the degradation

efficiency. The efficiency of HA degradation varied from 95% to 51% for UV-A and 97% to 47% for UV-C, respectively.

At 5 mg/L of HA concentration, the degradation efficiency is higher for the case of UV-C than that of UV-A, however, the difference is not significant. As the HA concentration increases from 8 mg/L to 14 mg/L, degradation efficiencies under UV-A irradiation showed higher values. This is due to the highest illumination intensities of UV-C. It shows that the activity of TiO_2 strongly depend on the light-illumination (energy per unit area) or the photon flux on the surface of the photo catalyst. Furthermore, a solution with a low concentration of HA with the same amount of hydroxyl radicals will have a higher degradation rate than a solution with a high concentration. Previous studies on trichloroethylene (TCE) reported that the reaction by-products generated during the photocatalytic reaction can also decrease the degradation rate (Bak et al., 2015).

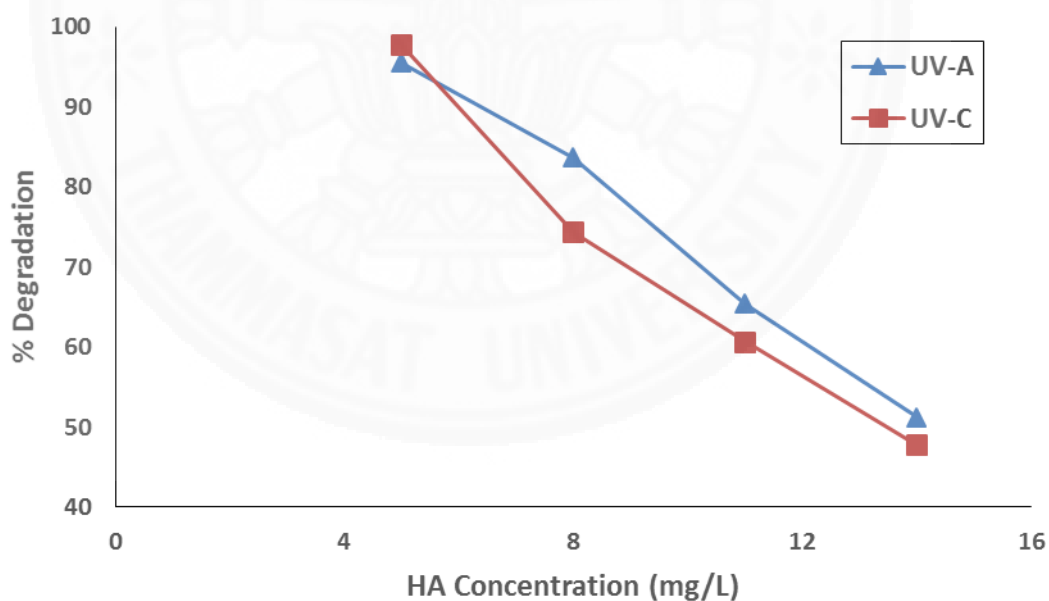


Figure 4.3 Effect of HA concentration on degradation by ZnO photocatalyst (ZnO dose 0.1 g/L, contact time 60min)

4.1.2.2 Effect of ZnO dose

In order to avoid the use of excess catalyst, it is necessary to find out the optimum loading for efficient degradation of pollutant. Figure 4.4 shows the results for degradation efficiency at different dosages of ZnO, when the initial concentration of HA at 5 mg/L. It was observed that the degradation efficiency is nearly consistent as the ZnO dose increases, for both irradiations. All the tested samples showed more than 90% degradation efficiency at 5 mg/L of HA concentration, regardless of the ZnO dose.

For the case of UV-A irradiation, the results of HA degradation continuously increased up to 0.8 g/L. This is due to an increase in the active sites available for absorption of UV irradiations and adsorption of HA molecules. Hence, it leads to produce large amounts of hydroxyl radicals, even though in this case is insignificant. When the amount of catalyst increases above a saturation level, the light photon absorption coefficient usually decreases. Therefore, it reduces the surface area of catalyst being exposed to light illumination and the photocatalytic efficiency (Chen et al., 2007). This phenomenon shows for ZnO dose at 1 g/L.

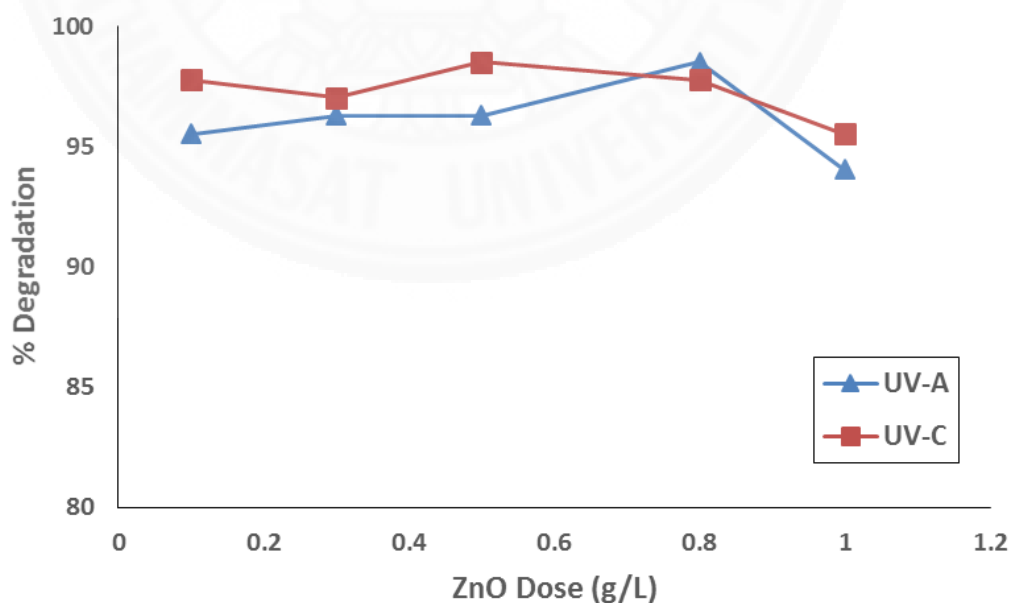
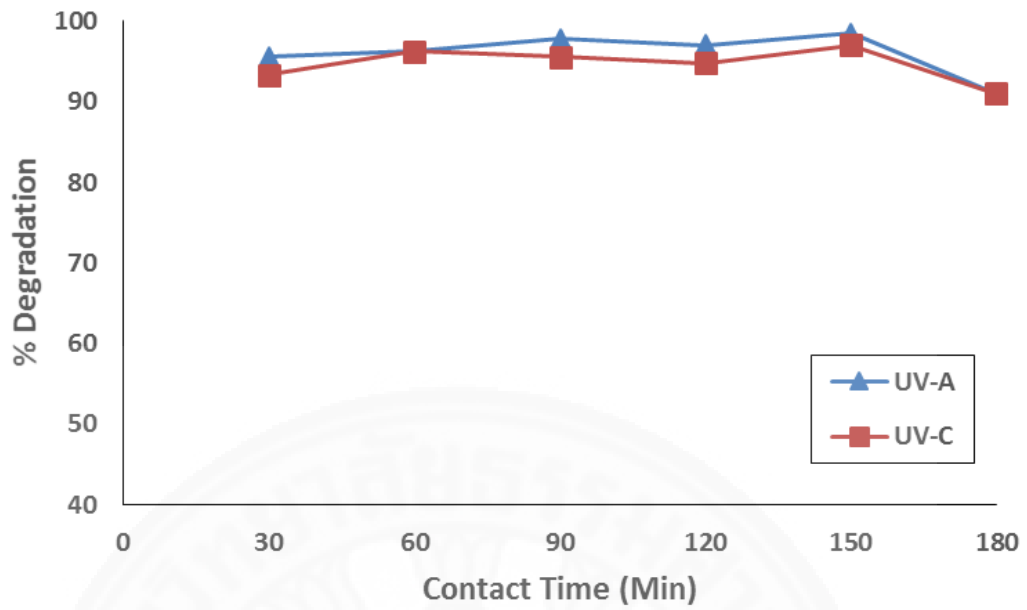


Figure 4.4 Effect of ZnO dose on degradation of HA (HA conc. 5 mg/L, contact time 60 min)

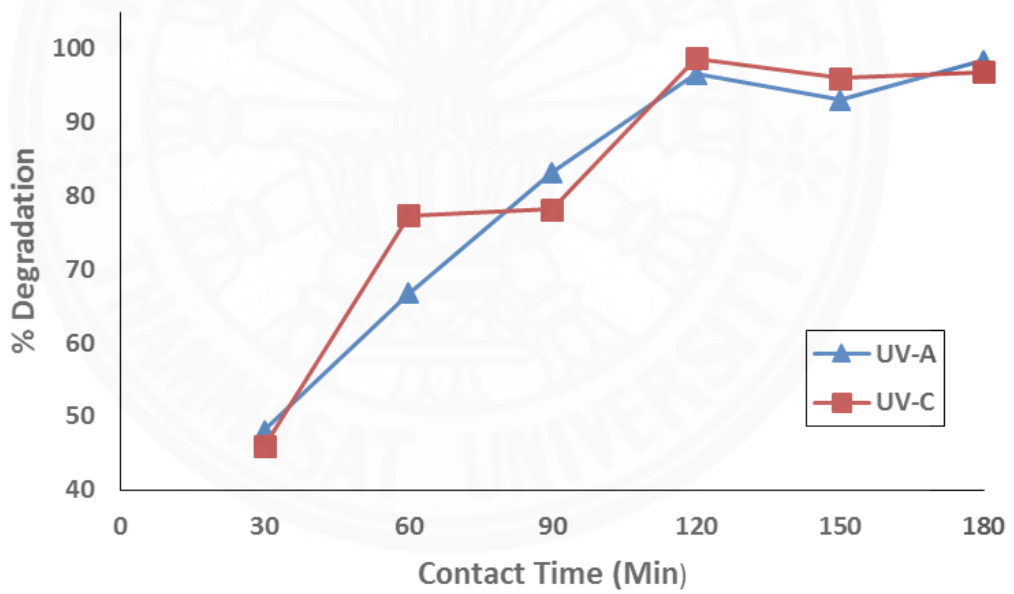
4.1.2.3 Effect of contact time

From the ZnO dose results, 0.5 g/L seemed to be the optimum dose. However, experiments were done for both 0.3 g/L and 0.5 g/L. It was observed that significant degradation at 60 min of contact time could be obtained by using 0.3 g/L. Therefore, 0.3 g/L was selected as the optimum of ZnO dose for experiments conducted here onwards.

Figure 4.5 (a) shows the effect of contact time for HA concentration of 5 mg/L. It shows that increasing the contact time from 30 min to 180 min increased degradation efficiency. The HA degradation for lower HA concentration at 5 mg/L only require about 30 min of contact time to reach more than 90% for both irradiations. After 30 min, the HA degradation seemed constant, with time. From the Figure 4.5 (b), the result shows rapid increase of degradation efficiency for higher concentration at 14 mg/L, especially at low contact time. Under UV-C irradiation, the HA degradation reached more than 70% in 60 min. However, it reached only up to 60% for the case of UV-A. The HA degradation seems constant in the range of 60 to 90 min under UV-C irradiation and increased at 120 min. However, under UV-A irradiation the HA degradation continuously increasing until 120 min. After 120 min of contact time, degradation efficiency remained nearly constant for both irradiations. The degradation efficiency was rapid at the beginning for high concentration because there were a large number of active sites available on the surface of the adsorbent. The number of sites decreased over time with the gradual occupation of sites by HA (Oskoei et al., 2016). The complex chemical structure of HA break down as the reaction of photocatalysis progresses. Therefore, the HA degradation efficiency increased as result of their internal bond are weakened, with time.



(a)



(b)

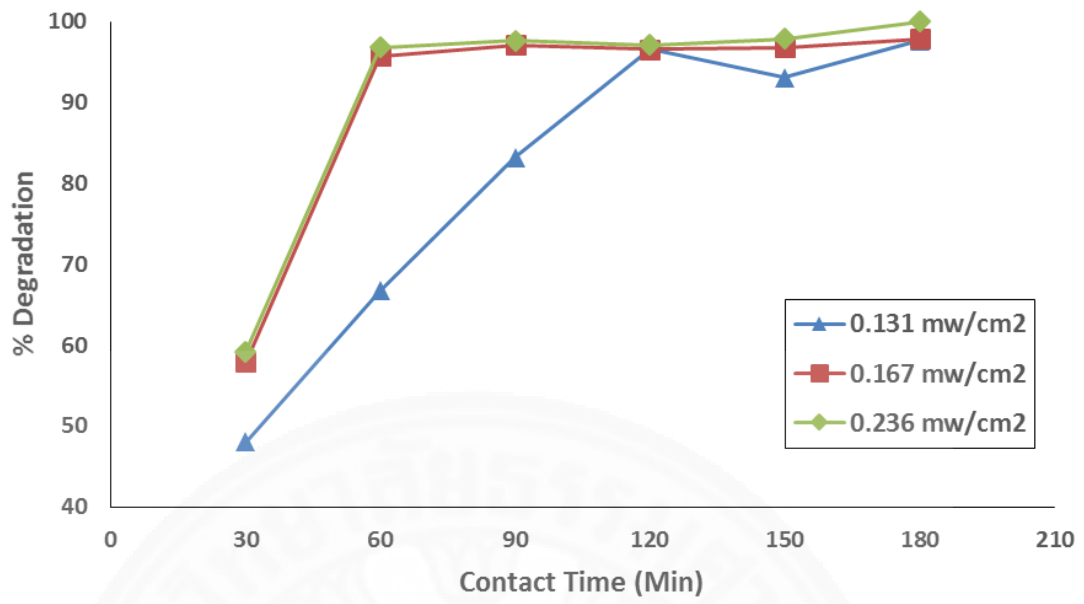
Figure 4.5 Effect of contact time on degradation of HA by ZnO photocatalyst
 (a) HA conc. 5 mg/L, ZnO dose 0.3 g/L
 (b) HA conc. 14 mg/L, ZnO dose 0.3 g/L

4.1.2.4 Effect of light intensity

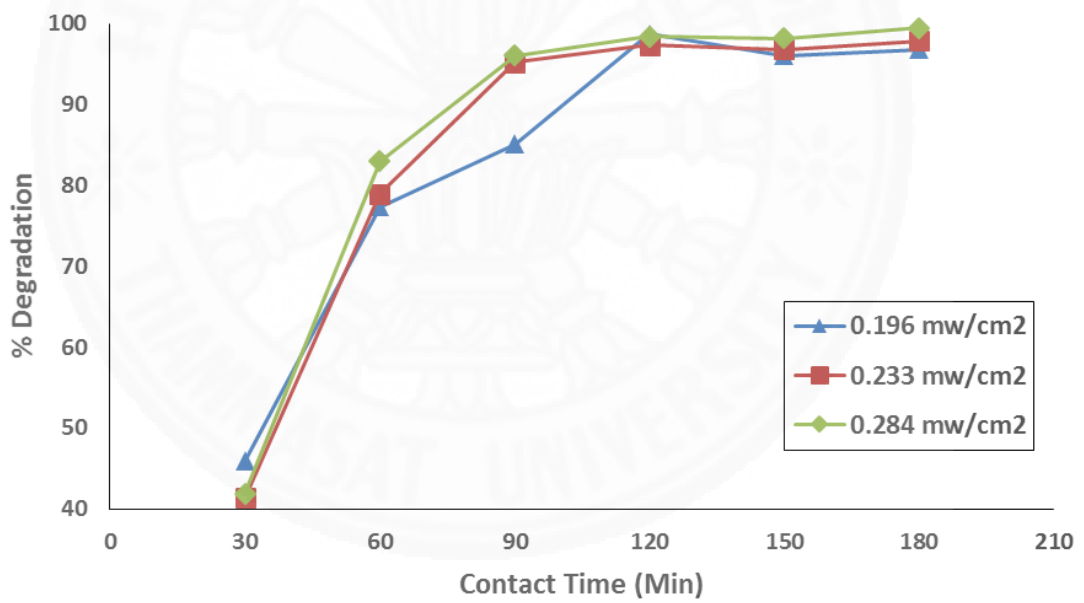
Figure 4.6 (a) and Figure 4.6 (b) show the effects of light intensity of 14 mg/L HA concentration for UV-A and UV-C, respectively, with time. In this study, contact time was varied from 30-180 min in order to find the effect of light intensity. Figure 4.6 (a) shows that under UV-A irradiation, different behaviors are observed in different light intensities. The lower intensity required 120 min of contact time to reach more than 90% of HA degradation. On the other hand, higher intensities required only 60 min of contact time. Figure 4.6 (b) shows lower intensity of UV-C irradiation required 120 min to reach more than 90% of HA degradation. For higher intensities required 90 min of contact time.

These graphs indicate that in terms of contact time, UV-A required lower contact time than UV-C to reach 90% of HA degradation. However, UV-C seemed to have higher degradation efficiency up to 150 min. For both irradiations, it is seen that HA degradation reached more than 90% within 120-180 min, regardless of the power of light intensity. Similar observation was obtained in a previous study by Bak et al. (2015), in an experiment done for photocatalytic oxidation of trichloroethylene under UV-A and UV-C irradiations. At higher intensities can result in higher electron-hole pair generation rate. It produces a positive hole and a free radical for higher electron-hole pairs. During this electron-hole pair generation, oxidation-reduction reactions take place (Zhang et al., 2011).

Degradation efficiency is increased with the increase of light intensity for all the tested cases. This is due to the fact that more radiation is absorbed by the catalyst surface for producing electron-hole pairs. This result in producing higher radical's which lead to higher degradation efficiency.



(a)



(b)

Figure 4.6 Effect of light intensity on degradation of HA by ZnO photocatalyst

(a) UV-A, HA conc. 14 mg/L, ZnO dose 0.3 g/L, contact time from 30 – 180 min

(b) UV-C, HA conc. 14 mg/L, ZnO dose 0.3 g/L, contact time from 30 – 180 min

4.1.3 Adsorption

Figure 4.7 indicates the percent adsorption and photodegradation under UV-A and UV-C irradiation at different time. Initially, the adsorption process occur where the HA molecules are attached onto the surface of ZnO. This step is followed by photodegradation process. ZnO lower bandgap (3.3 eV), affect the photodegradation process since it provides higher concentration of hydroxyl ions to react with holes to form hydroxyl radicals. Hydroxyl radical is considered to be responsible for oxidation decomposition of organic compound. However, agglomeration and accumulation of ZnO might be occurred in the absence of irradiation.

In addition to the above experiments, photolysis of UV-A and UV-C was investigated at 14 mg/L of HA concentration for a contact time of 180 min. The values for percentage of HA degradation were 77% and 79%, under UV-A and UV-C irradiations, respectively. Therefore, it indicates that photolysis place a role in HA degradation. HA degradation efficiency can be further enhanced by photodegradation.

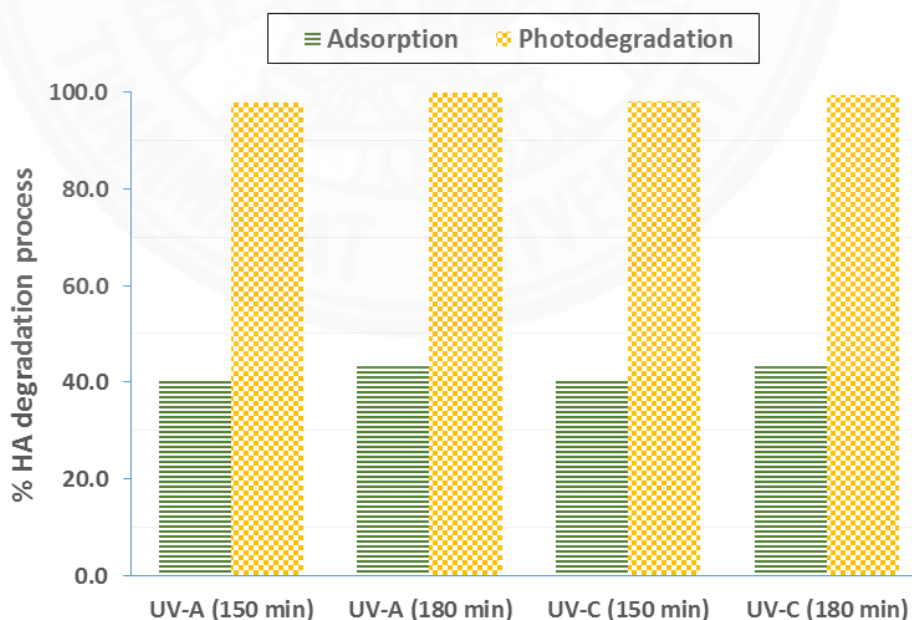


Figure 4.7 Percent adsorption and photodegradation under UV-A and UV-C irradiation at different time (HA conc. 14 mg/L, ZnO dose 0.3 g/L, contact time 180 min)

4.1.4 Reusability of catalyst

In order to study the reusability of the catalyst, centrifugation separation method was used. Photocatalytic experiments were performed at 14 mg/L HA and 0.3 g/L ZnO, with 180 min of contact time. The ZnO was reused up to three cycles with consistent activity. Similar studies were done on TiO₂ for five cycles (Putri et al., 2015). After three cycles of reusability, the percentages of degradation obtained were 88% for UV-A and 76% for UV-C, respectively, as shown in Figure 4.8 below. With higher number of cycles, the percentage of catalyst recovery decreased. The ZnO dissolution might have occurred within the process resulting in reduced catalyst recovery.

After first cycle, it is seen that under UV-C irradiation the HA degradation becomes lower compared to UV-A. This is due to the capability of ZnO nanoparticles to agglomerate due to their high surface energy. This can be supported by BET results in Table 4.1. It shows that the surface area of ZnO decreased after 180 min photocatalytic process. The decrease of HA degradation might occur from the photocorrosion effect, which affected catalyst to a large extent. Huang et al. (2009), showed similar result on Cu₂O where the photocorrosion rate was rapid in catalyst as against their micron sized counterparts. Therefore, three cycles of reusability is suggested to be acceptable from the experiments of this study.

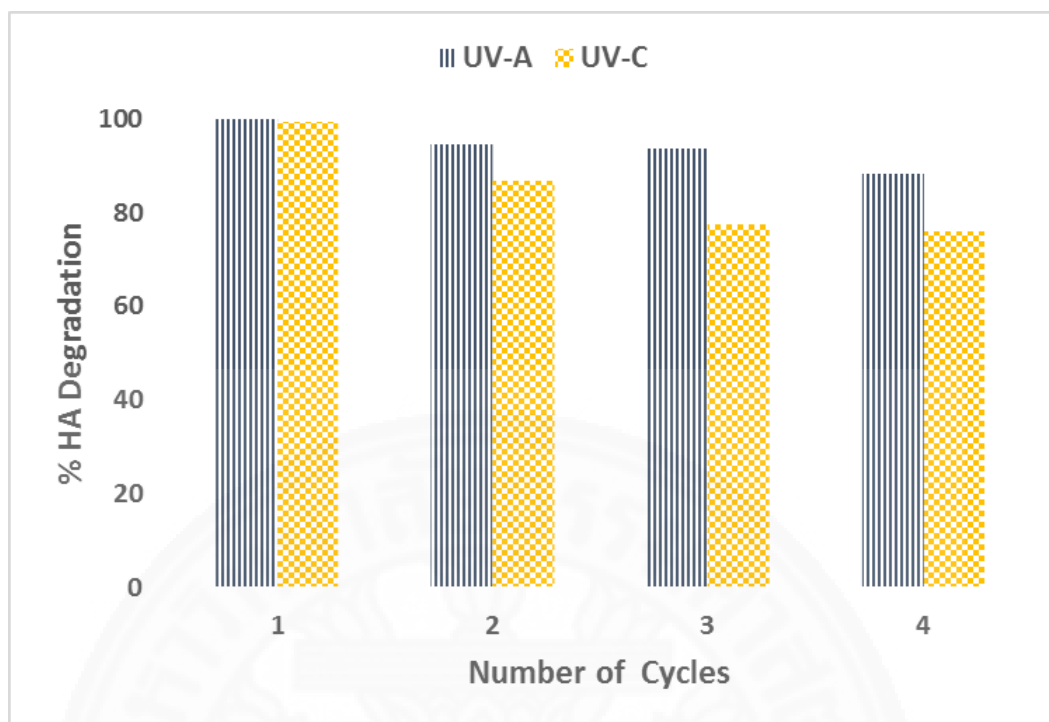


Figure 4.8 Catalyst reusability under UV-A and UV-C irradiation
(HA conc. 14 mg/L, ZnO 0.3 g/L, contact time 180 min)

4.2 HA Degradation by TiO₂ Photocatalyst

4.2.1 Characteristic of TiO₂ as a catalyst

4.2.1.1 XRD Analysis

The catalyst characterization analysis of TiO₂ was performed by X-ray diffractometer. The testing conditions were at step angle 0.02°; count time 0.5 sec; D-, R- and S-slits 1°, 1/2° and 1/4°, respectively, target type: Cu; tube voltage 40 kV; current 30 mA. It can be seen that TiO₂ used in this experiment is formed of two phases, anatase and rutile. It can be indicated by characteristic of XRD pattern in Figure 4.9. The diffraction pattern indicated that the rutile phase showed diffraction peaks at 27°, 36° and 55°. Whereas, the diffraction peaks at 25° and 48° indicating for the the anatase phase (Thamaphat et al., 2008).

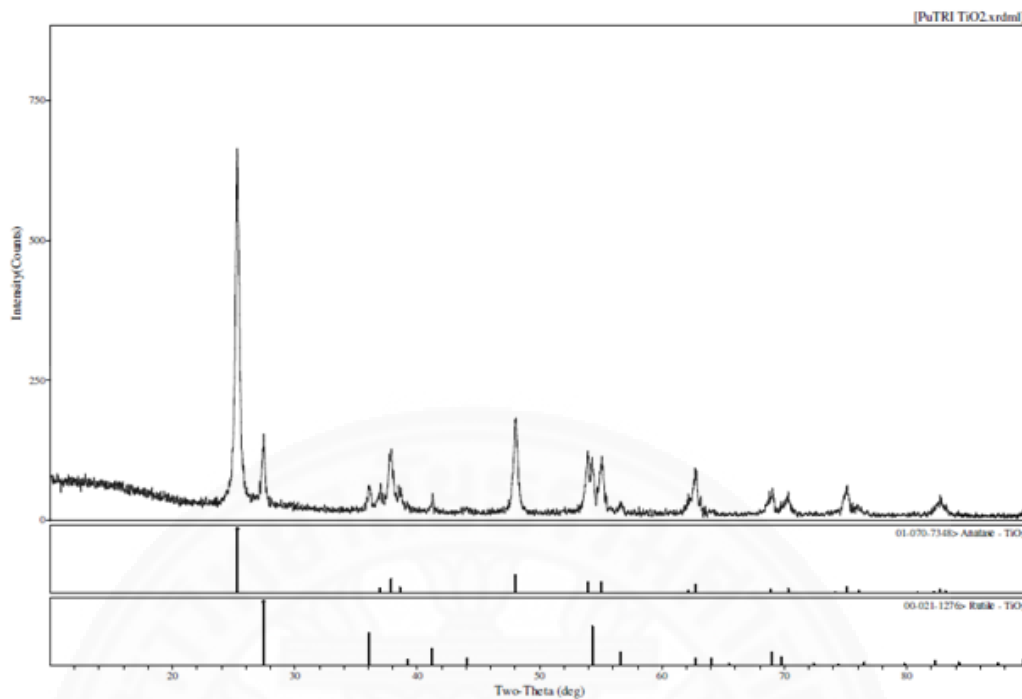


Figure 4.9 X-ray diffraction pattern of TiO₂

4.2.1.2 FT-IR Analysis

The composition quality of the TiO₂ was characterized by Fourier transform infrared (Thermo Nicolet 6700 FT-IR spectrophotometer) spectroscopy in the mid-infrared range (400–4000 cm⁻¹). The sample was ground together with potassium bromide (KBr) to a fine powder and the mixture was transferred to the compression die. It was placed under high pressure until a pellet was formed. Figure 4.10 shows the FT-IR spectra of as prepared the TiO₂ initial and after photocatalytic treatment for UV-A and UV-C, respectively. It is observed in the graph that the initial TiO₂ nanoparticles have different peaks formed. The peak of initial TiO₂ at 3442.64 cm⁻¹ corresponds to O—H stretch region. A broad band at 1635.31 cm⁻¹ is characteristic of O—Ti—O bond and narrow adsorption band is observed due to Ti=O bending region. The sharp peak at 1384.29 cm⁻¹ is due to the scissoring of —CH₂ or the symmetric deformation of the —CH₃ group. TiO₂ oxides generally give absorption bands in fingerprint region below 1000 cm⁻¹, which is assigned to arise from interatomic vibrations at 499.25 cm⁻¹.

From Figure 4.11, FT-IR spectra under UV-A shows similar graph pattern with UV-C. The peak of O-H stretching vibration shows the interaction between the molecules, which effected the shifting of peak at 3442.64 cm^{-1} of initial to 3396 cm^{-1} for both irradiations. The molecules of H_2O released as a result of adsorption of HA onto the TiO_2 through O-H bond. Similar phenomenon is appeared for H-O-H bending vibration. The shift of peak occurred at 1635.31 cm^{-1} to 1629 cm^{-1} for both irradiations. It shows that the energy of O—Ti— O bond and narrow adsorption bond decrease. Compared to the initial, the peak at 1384.29 cm^{-1} which corresponds to the scissoring of $-\text{CH}_2$ or the symmetric deformation of the $-\text{CH}_3$ group disappeared. The new absorption peak appeared at 621.36 cm^{-1} for both irradiations, corresponding to $=\text{C-H}$ bending vibration, this occurred due to the HA degradation by products adsorbed on the surface of TiO_2 .

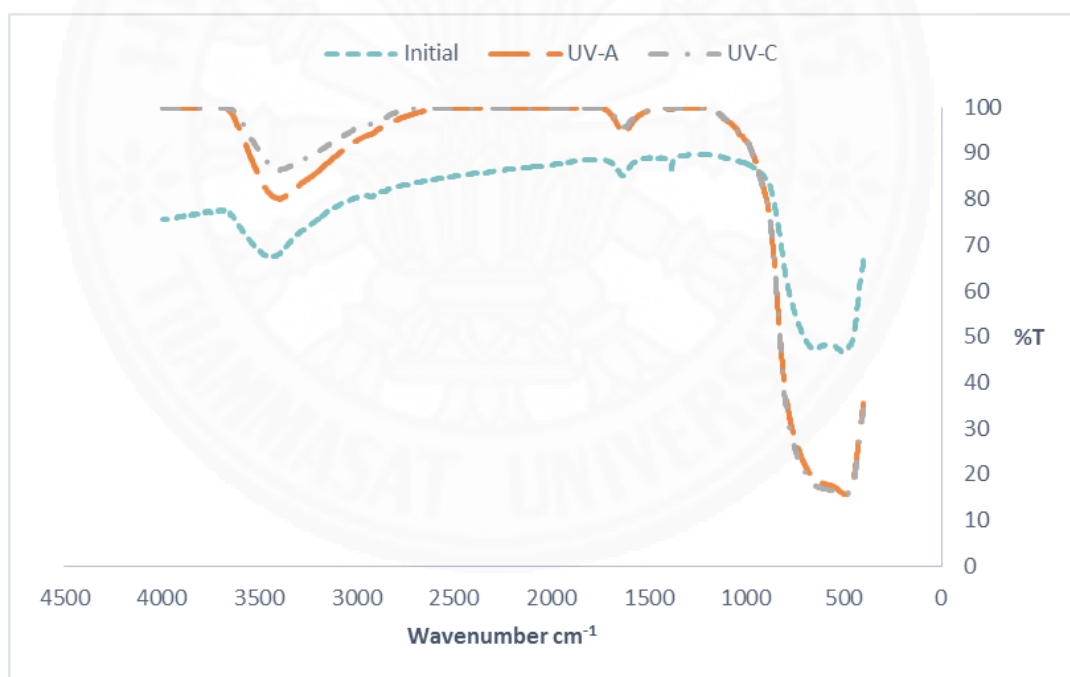


Figure 4.10 FT-IR spectra of TiO_2

4.2.1.3 BET Analysis

The Table 4.3 indicates properties of TiO₂ based on BET analysis before and after photocatalytic process. Similar tendencies of the results were obtained as the BET results of ZnO. After the photocatalytic process, the agglomeration of the catalyst results in lower specific surface area. The cause for this agglomeration is due to hydrogen bonding as explained previously for the case of ZnO.

Table 4.3 Properties of TiO₂ based on BET analysis

Parameter	Specific surface area (m²/g)	Total pore volume (cm³/g)	Pore diameter (nm)
TiO ₂ (Initial)	52	0.026	2.008
TiO ₂ (UV-A)	47.30	0.023	1.974
TiO ₂ (UV-C)	49.59	0.025	1.989

4.2.1.4 XRF Analysis

From Table 4.4, the elements of TiO₂ initial and after treatment were observed by XRF analysis. The initial of TiO₂ shows that 99.8% containing of the purity of TiO₂. Meanwhile, for TiO₂ after treatment it was found that several elements attached on the TiO₂ surface. However, the elements SiO₂, Fe₂O₃, ZnO, and CaO attached on the TiO₂ surface in relatively small amount, less than 1%. When comparing with the elements inside HA as shown in Appendix.1, the possibility of the attachment of SiO₂, Fe₂O₃, ZnO, and CaO may be due to HA composition.

Table 4.4 TiO₂ elements based on XRF analysis

Element	TiO₂ (Initial)	TiO₂ (UV-C)
TiO ₂ (%)	99.8	99.3
Cl (%)	0.128	-
SiO ₂ (%)	-	0.462
SO ₃ (ppm)	541	-
Fe ₂ O ₃ (ppm)	-	966
ZnO (ppm)	-	989
CaO (ppm)	-	366

4.2.2 Pertinent factors of HA degradation

4.2.2.1 Effect of HA concentration

The effect of HA concentration on degradation is indicated from Figure 4.11, the degradation of HA decreased from 74 to 47% for UV-A and 96 to 58% for UV-C, respectively, when concentration is increased from 4 to 14 mg/L. It can be explained from previous studies which show similar results for the photocatalytic oxidation of other organic compounds. Palmer et al. (2002), reported that the decreasing of the degradation efficiency is because of the fixed active site number at the TiO₂/H₂O interface. Thus, at low HA concentrations, an increased amount of water molecules will be adsorbed onto the available TiO₂ particles, generating hydroxyl radicals and resulting in a fast oxidation progression. In contrast, at increased HA concentrations, there is a lower ratio of water molecules to free active sites, since the amount of active sites are similar. Subsequently, competitive adsorption between the HA and water molecules progresses and results in a decrease in the degradation rate.

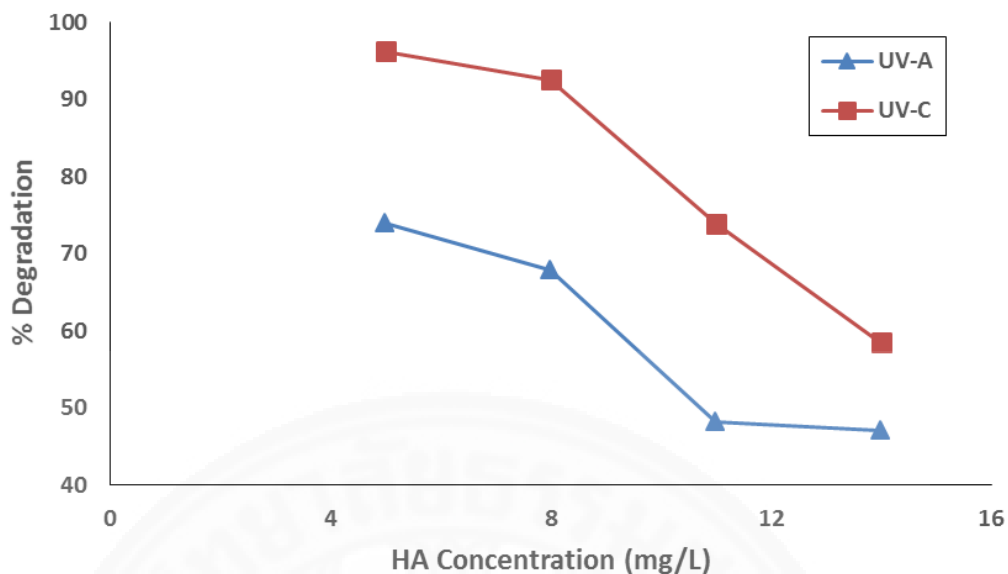


Figure 4.11 Effect of HA concentration on degradation by TiO_2 photocatalyst (TiO_2 dose 0.1 g/L, contact time 60min)

4.2.2.2 Effect of TiO_2 dose

Figure 4.12 shows the effect of TiO_2 dose on HA degradation at 5 mg/L initial concentration and with a contact time of 60 min. It was observed that the HA degradation under UV-C irradiation reached more than 90% for all dosages of TiO_2 . Moreover, almost constant values were obtained for degradation efficiencies of UV-C. For the case of UV-A irradiation, the degradation efficiency was considerably low at lower dosage of TiO_2 . This behaviour is similar to that of the Figure 4.11, which explained about the effect of HA concentration previously. This is due to the dose of TiO_2 at 0.1 g/L, under UV-A irradiation less powerful to generate the hydroxyl radicals which can degrade the HA. However, when the TiO_2 dose increasing at 0.3 g/L, the HA degradation increased. This is due to the availability of more catalyst surfaces for absorption of UV irradiations, which resulted in producing higher amount of hydroxyl radicals. For higher dosage from 0.5 g/L to 1 g/L, the HA degradation seemed constant under UV-C irradiation and slightly decreased at 0.8 g/L under UV-A irradiation. The decrease of HA degradation rate might be caused not only by photodegradation reaction but also by the adsorption of HA on TiO_2 surface. Further, the presence of TiO_2 particles in suspension causes the dispersion of radiation. At the

high TiO_2 concentration the penetration depth of radiation into the layer of suspension may be limited, leaving part of the solution not irradiated. During the photocatalytic process, large amounts of particle aggregation may also occur, thus reducing the catalyst surface.

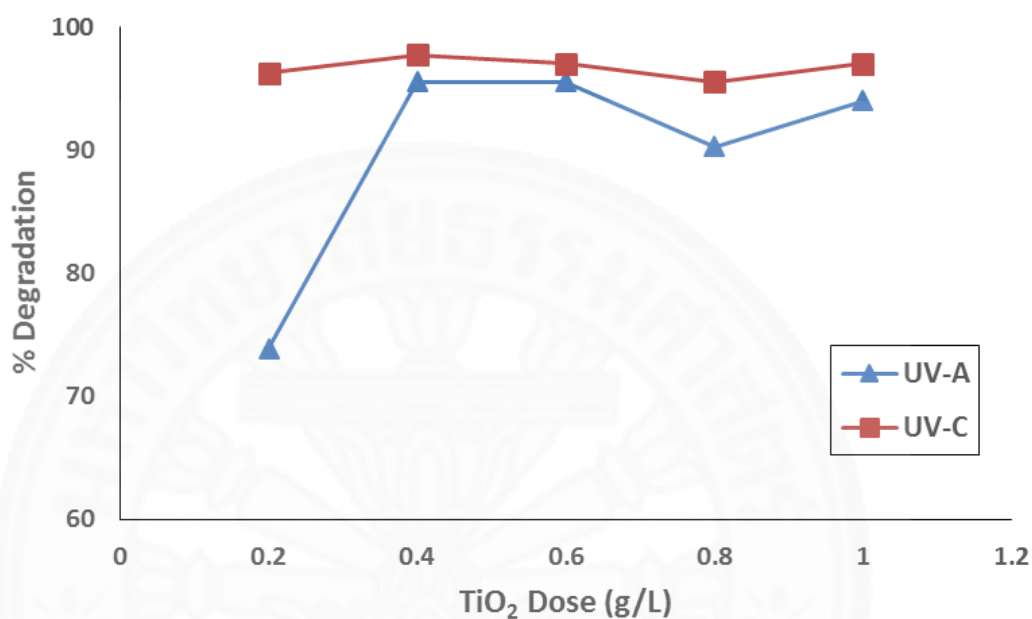


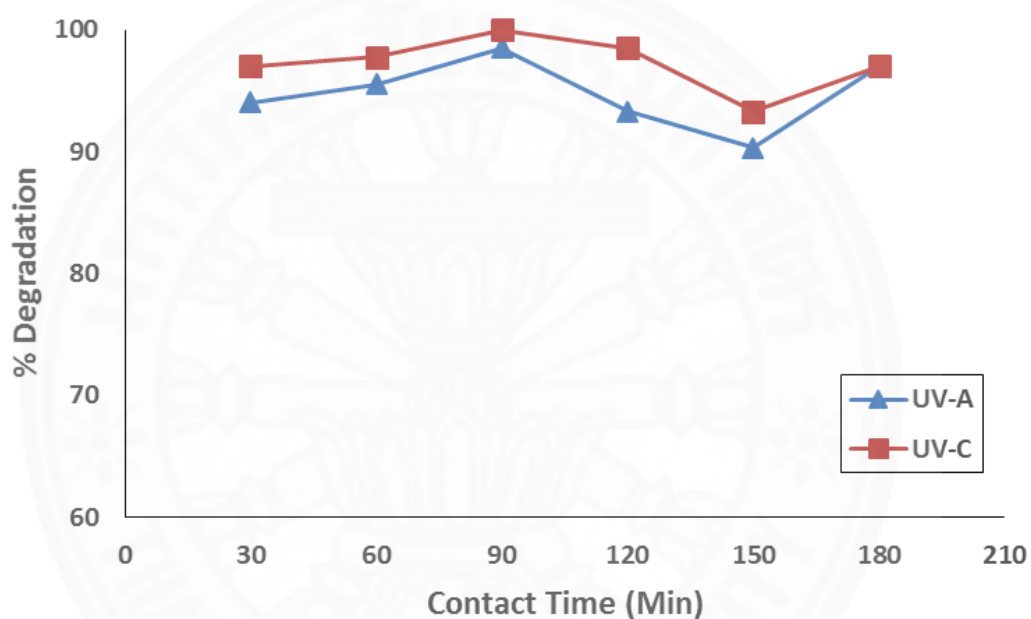
Figure 4.12 Effect of TiO_2 dose on degradation of HA (HA conc. 5 mg/L, contact time 60 min)

4.2.2.3 Effect of contact time

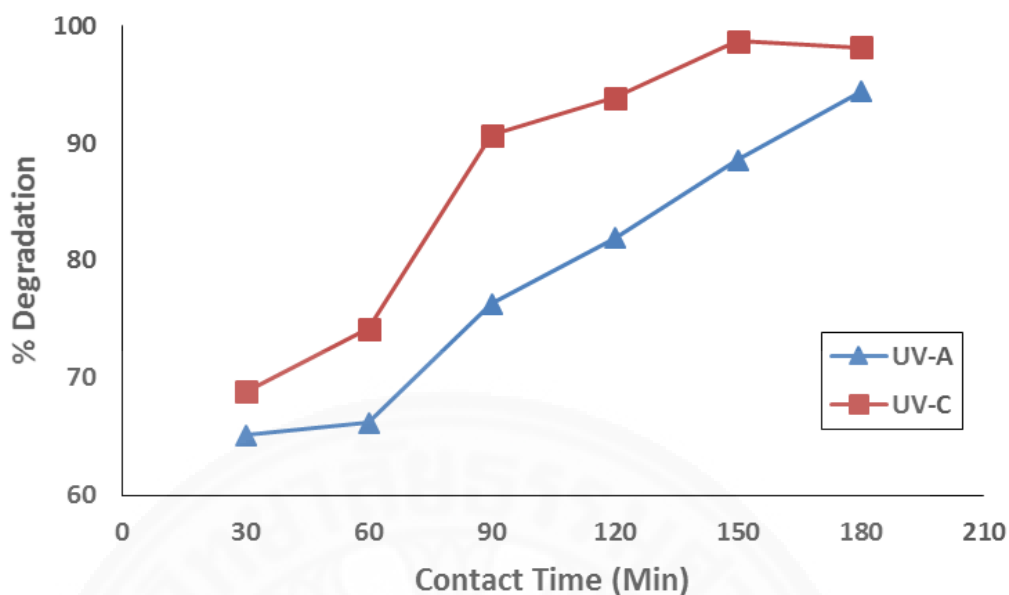
Figure 4.13 (a) shows the effect of contact time for HA concentration of 5 mg/L. The HA degradation for lower concentration reached more than 90% within a very short period of 30 min under UV-A and UV-C irradiations. After 30 min, the HA degradation seemed insignificant, with time. From the Figure 4.5 (b), the result shows rapid increase of degradation efficiency for higher concentration at 14 mg/L, especially at low contact time. Under UV-C irradiation, the HA degradation reached more than 70% within 60 min, whereas, UV-A reached more than 60% only. The HA degradation continuously increased from 60 to 180 min under UV-C irradiation. Similar behavior was observed for the case of UV-A. This is due to the complex chemical structure of HA break down as the reaction of photocatalysis progresses.

Therefore, the HA degradation efficiency increased as result of their internal bond are weakened, with time.

In both lower and higher concentrations, UV-C irradiation showed higher performance in HA degradation than that of the UV-A case. This is because the UV-C irradiation consists of higher energy to provide higher electron-hole pair generation rate which leads to produce higher number of hydroxyl radicals.



(a)



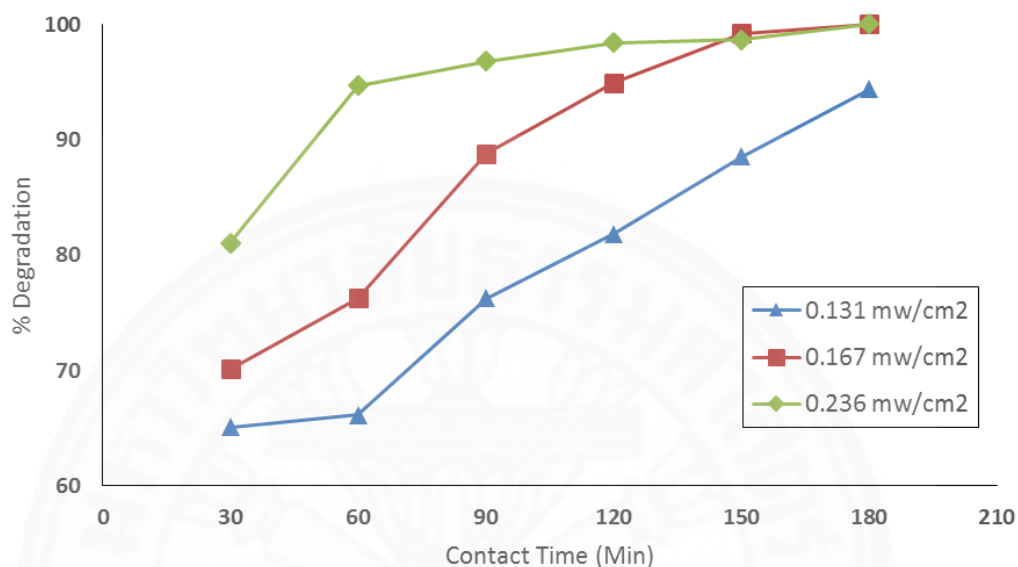
(b)

Figure 4.13 Effect of contact time on degradation of HA by TiO₂ photocatalyst
 (a) HA conc. 5 mg/L, TiO₂ dose 0.3 g/L
 (b) HA conc. 14 mg/L, TiO₂ dose 0.3 g/L

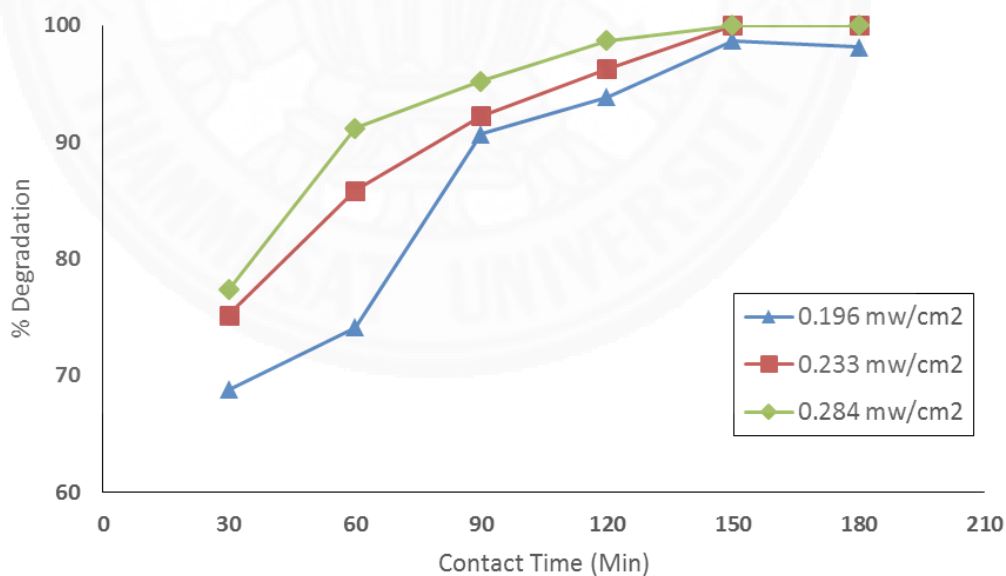
4.2.2.4 Effect of light intensity

Figure 4.14 (a) and Figure 4.14 (b) shows the effects of light intensity for UV-A and UV-C, respectively. For lower light intensities, UV-C lamp shows more efficiency in degradation of HA than that of UV-A. However, in higher light intensities, UV-A shows higher performance of HA degradation. This is due to the different activation amount of TiO₂ phases. TiO₂ phases consist of two types, which are anatase (approximately 80%) and rutile (approximately 20%). The rutile phase is activated in higher wavelength, according to previous studies (Pansamut et al., 2013). The band gap of TiO₂ is generally in range of 3.0–3.2 eV, wavelength is about 400 nm. This means that UV light irradiation with a wavelength lower than 400 nm begins a photo-reaction. The characteristics of TiO₂ are the more powerful oxidative power of the valence band holes than the reducibility of photo-induced electrons. The TiO₂ has oxidation power, 3.2 eV for anatase and 3.0 eV for rutile, considering the approximately 3.0 eV from the hydrogen reference potential and approximately 1.2

eV from oxidation potential of water (Chen et al., 2007). In higher intensities, effects of wavelength is higher in UV-A, which results in higher degradation by rutile phase. Therefore, UV-A show higher performance at higher light intensities.



(a)



(b)

Figure 4.14 Effect of light intensity on degradation of HA by TiO₂ photocatalyst
 (a) UV-A, HA conc. 14 mg/L, TiO₂ dose 0.3 g/L, contact time from 30 – 180 min
 (b) UV-C, HA conc. 14 mg/L, TiO₂ dose 0.3 g/L, contact time from 30 – 180 min

4.2.3 Adsorption

Similar to the explanation mentioned in section 4.1.3, the process is initiated by adsorption which is followed by photodegradation. In order to determine the process of HA degradation, experiments of adsorption were carried out in the dark at optimum condition. Higher contribution from adsorption can be seen in Figure 4.15. More than 50% of HA was adsorbed on TiO₂ surface. As a result, HA is might be composed of at least two components, one adsorbing easily at the TiO₂ surface, the other one does not adsorb at all or adsorbs to a very limited extent. Photodegradation reaction of such complicated compounds as HA, which has large size and contain more functional groups per molecule, is not possible to occur in one stage (Palmer et al., 2002). Intermediate species formed during degradation may desorb from the surface with some delay. This can be supported by TOC solid phase results in Table 4.7. It is can be seen that by-products of HA were attached on the catalyst surface. Furthermore, FT-IR spectra in Figure 4.10 shows that a new peak was formed as a by-products of HA degradation were generated.

Similar to that of the ZnO case which was described previously in 4.1.3 section, photolysis of UV-A and UV-C was investigated at 14 mg/L of HA concentration for a contact time of 180 min. Thus, it is proved that the photolysis can cause degradation of HA. Further, HA degradation efficiency can be enhanced by photodegradation.

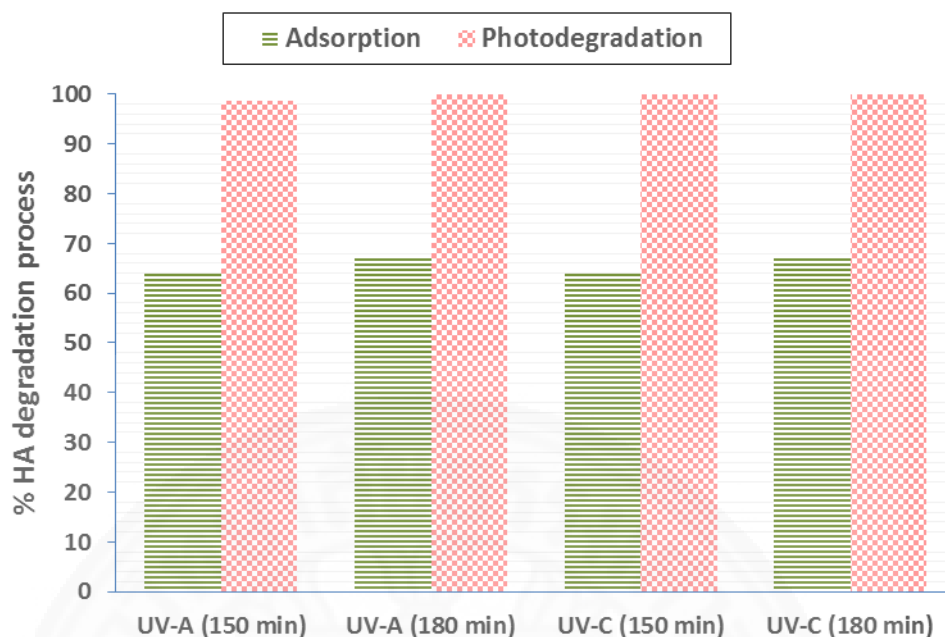


Figure 4.15 Percent of adsorption and photodegradation under UV-A and UV-C irradiation at different time (HA conc. 14 mg/L, ZnO dose 0.3 g/L, contact time 180 min)

4.2.4 Reusability of catalyst

In this experiment, TiO_2 was separated from the sample by using centrifuge. The TiO_2 was reused for five cycles under identical experimental conditions to investigate the efficiency of reusability of catalyst. After five reuses of the TiO_2 , there is a decrease in the degradation efficiency of the catalyst as seen in Figure 4.16. This is due to the high molecular weight compound of HA, with a large number of functional groups per molecule. The aggregation of the HA is occurred in this process. This may affect to the reduction of degradation percentage (Palmer et al., 2002). After 5 cycles of reusability, the percentages of degradations obtained were 74% for UV-A and 57% for UV-C, respectively. However, the reusability of the catalysts is essentially beneficial when considering the commercial applications (Mohammad et al., 2011). As previously mentioned in reusability of ZnO catalyst, same behavior were observed, where both catalysts consist of thorough photochemical stability.

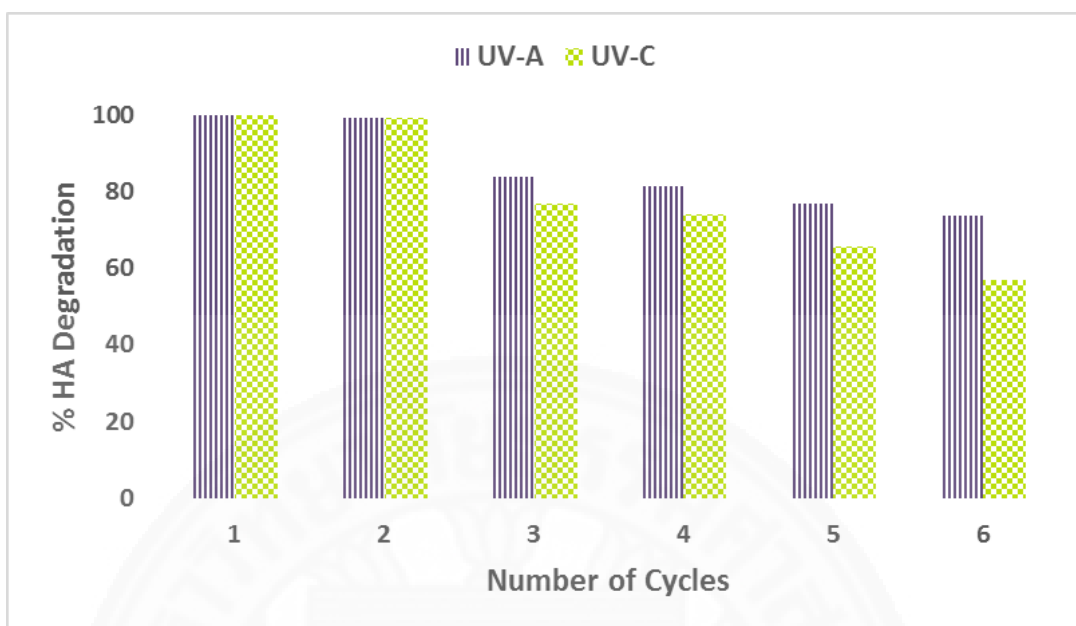
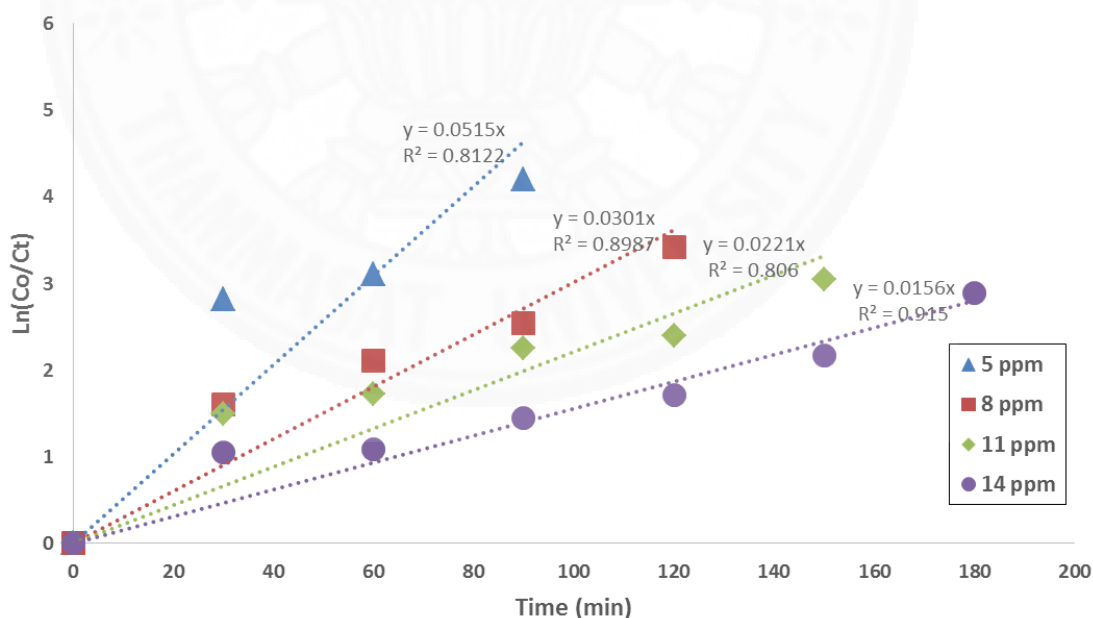


Figure 4.16 Catalyst reusability under UV-A and UV-C irradiation
(HA conc. 14 mg/L, ZnO dose 0.3 g/L, contact time 180 min)

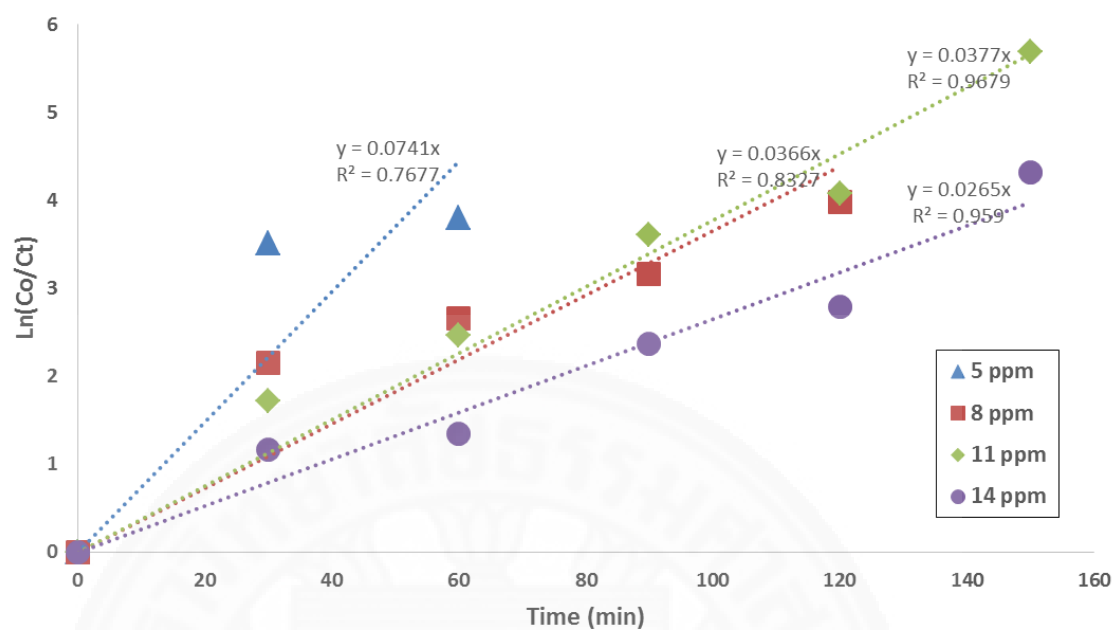
4.3 Pseudo-first order Kinetics

Figure 4.17 and 4.18 were obtained by plotting $\ln(C_0/C_t)$ versus time as mentioned previously from Equation 4. K' values were obtained from the tangents of these plotted graphs. Then half-life ($t_{1/2}$) of photocatalysis was determined by Eq.(5). The variables were summarized from Table 4.5 and 4.6. It is shown that the accuracy of the plotted graphs increase with increase of initial concentration for both TiO_2 and ZnO photocatalysts. From Figure 4.17 and 4.18 shows the slopes of plots which express the photodegradation rate constants. The experimental results for different initial HA concentrations indicated sufficient accuracy with the first order reaction as shown from Eq.(2). Therefore, the first order kinetics expression can be applied to investigate the photocatalytic reaction process. The correlation coefficients obtained for both TiO_2 and ZnO catalysts indicate good fitting of experimental data to that of the kinetics equation. Similar results were obtained previously by Akpan and Hameed (2011), on photocatalytic degradation of 2,4 dichlorophenoxyacetic acid by Ca-Ce- TiO_2 composite photocatalyst.

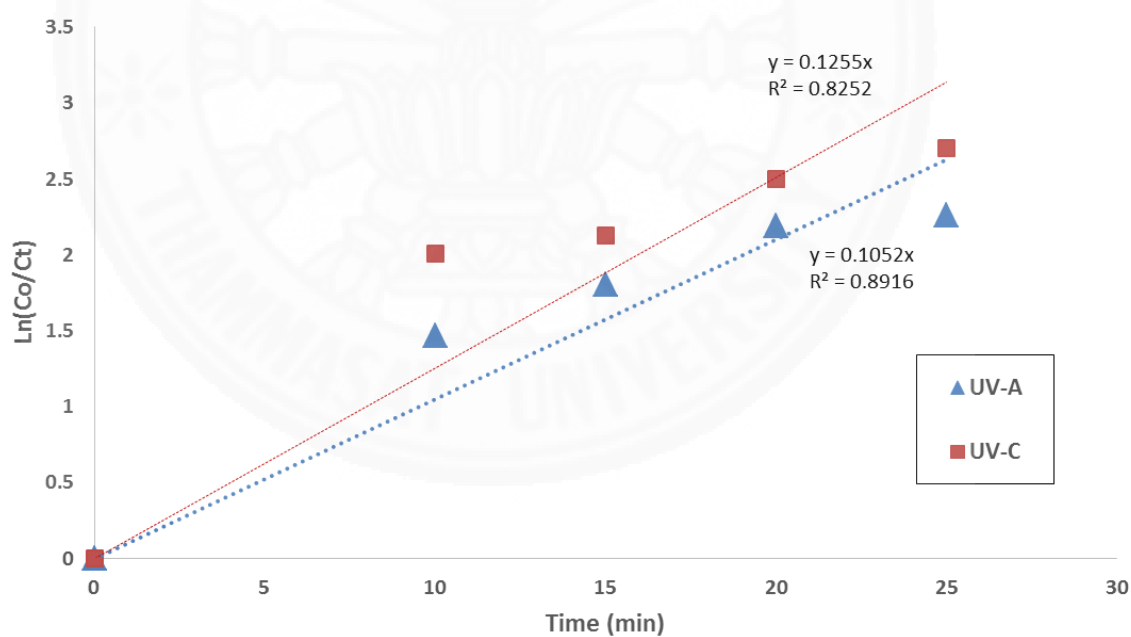
It is evident that photocatalytic activity is more profound when the initial concentrations of pollutant are lower. The results in Figure 4.17 and 4.18 confirm that in lower HA concentrations, the photocatalytic activity increases. This can be due to the reduction formation of hydroxyl radicals with increasing of HA. Other than generating the oxidizing species, oxygen involve in carrying the photogenerated charge at the semiconductor. It is influenced to a certain level to the surface properties of the semiconductor, depending on surface hydroxyl groups and on adsorbed charge molecules. Similar result was obtained by Yu et al. (2008) for the influence of fluoride on photoactivity. Furthermore, the effect of contact time at lower HA concentration was also carried out from 5 – 25 min. It can be seen in Figure 4.17 (c) and 4.18 (c) that at lower concentration of 5 mg/l of HA at contact time ranging from 30 – 180 min, the slopes of the trend lines were higher than in the cases for lower contact time. At lower concentration, the degradation is faster initially as seen from Figure 4.17 (c) and 4.18 (c). At higher contact time, the equilibrium time is already reached (5 mg/L). Similar observations were found for both catalyst TiO₂ and ZnO.



(a)



(b)



(c)

Figure 4.17 Kinetics of HA degradation by TiO₂ photocatalyst ($\ln(Co/Ct)$ vs. t) at various initial HA concentration (TiO₂ dose: 0.3 g/L)
 (a) UV-A; (b) UV-C; (c) HA conc. 5 mg/L, at lower contact time (5 - 25 min)

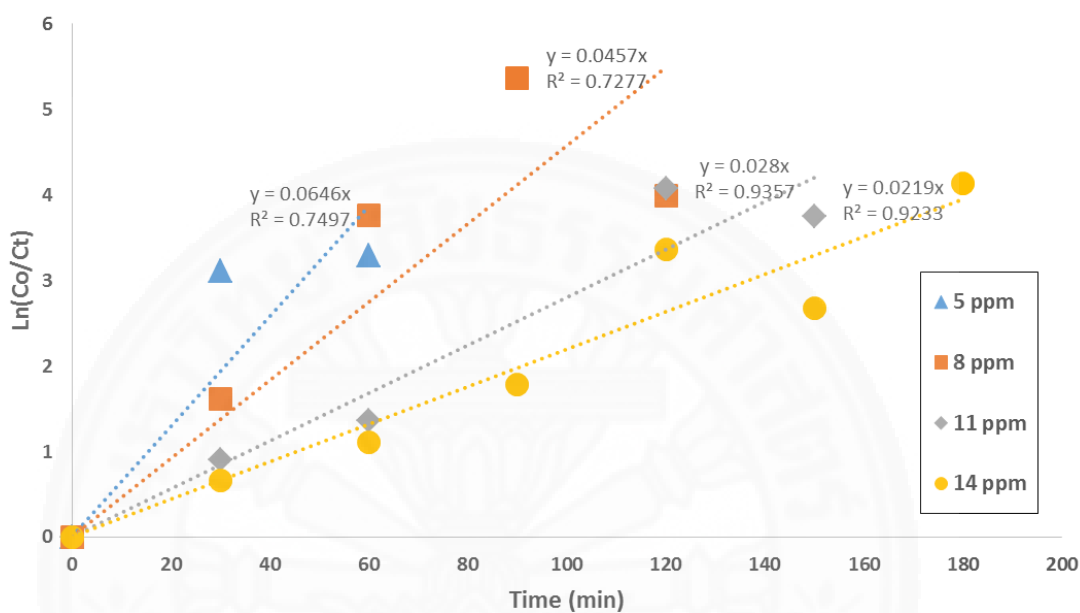
Table 4.5 Kinetic parameters of HA degradation by TiO₂ photocatalyst at various initial HA concentration

Co	UV-A			UV-C		
	K'	R ²	t _{1/2}	K'	R ²	t _{1/2}
5	0.052	0.812	13.46	0.074	0.768	9.35
8	0.030	0.899	23.02	0.038	0.833	18.38
11	0.022	0.806	31.36	0.037	0.968	18.93
14	0.016	0.915	44.42	0.027	0.959	26.15

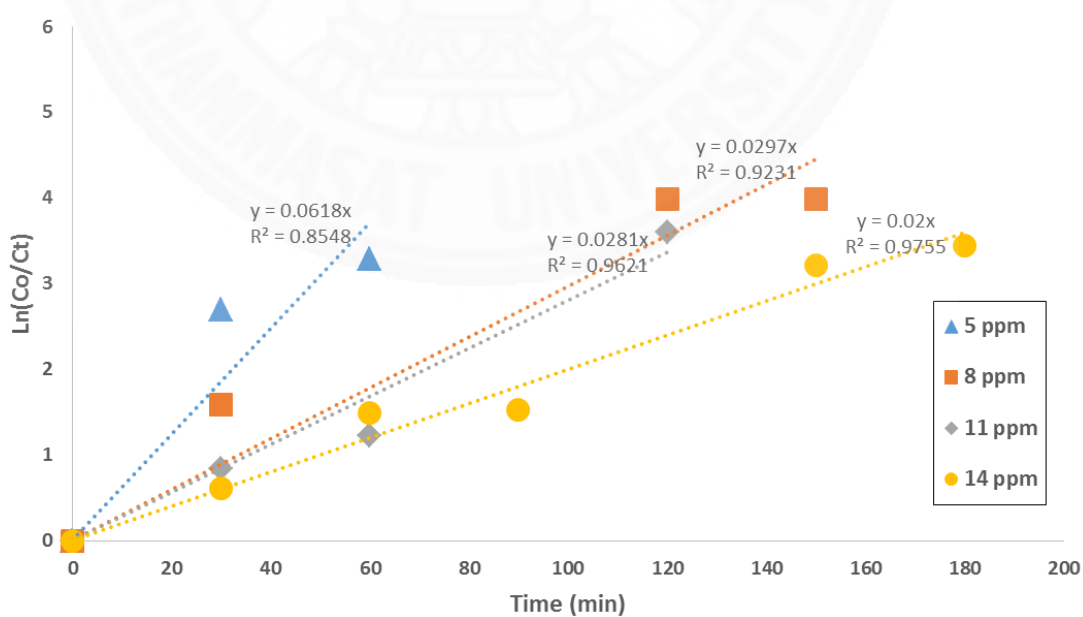
Comparing the slopes of the graphs shown in Figure 4.17 and 4.18 show that lower HA concentrations of HA lead to higher slopes. The values for K' which represents the slope, are mentioned in Table 4.5 and 4.6. Comparing the K' values for the two cases of TiO₂ and ZnO may lead to illustrating the efficiency of the catalysts. It is clearly seen from Table 4.5 and 4.6 that the K' values are higher in ZnO for all UV-A cases. However, the values are higher in TiO₂ for all UV-C cases. It shows that the ZnO performs better in UV-A irradiation while TiO₂ in UV-C irradiation. It is reported previously that ZnO can exhibit higher UV absorbance than TiO₂ within the wavelength range of 320-385nm under UV-A irradiation. This phenomenon occur due to effect of UV-A irradiation on ZnO surface redox reaction, in which higher levels of hydrogen peroxide were generated in UV-irradiated ZnO suspensions compared to TiO₂ in the absence of added electron donors under this condition (Han et al., 2012).

Moreover, TiO₂ show higher performance under UV-C irradiation in this study. Similar observation was made previously where UV-C lamp resulted in highest apparent rate constant values for TiO₂. The reason may be due to the highest illumination intensities of UV-C. It shows that the activity of TiO₂ strongly depend on the light-illumination (energy per unit area) or the photon flux on the surface of the photo catalyst. In this study, comparatively the order of degradation was highest in UV-C which was then followed by UV-A. In a study by Majid et al. (2011), it was also reported that TiO₂ under UV-C irradiation can be successfully used for the treatment of Rhodamine B contaminated wastewater. The band gap values of ZnO for

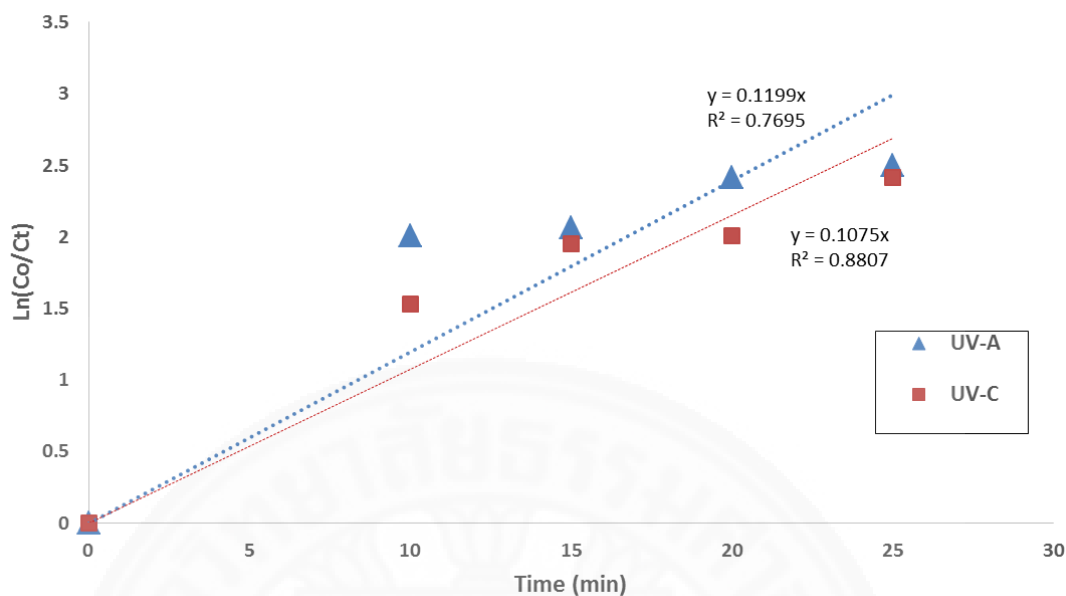
UV-A and TiO₂ for UV-C are reported previously as 3.3 eV and 3.0-3.2 eV, respectively. However, the effect from other parameters was more profound than that from band gaps. Therefore, the effect from band gaps for degradation results may be not much different.



(a)



(b)



(c)

Figure 4.18 Kinetics of HA degradation by ZnO photocatalyst ($\ln(Co/Ct)$ vs. t) at various initial HA concentration (ZnO dose: 0.3 g/L)
 (a) UV-A; (b) UV-C; (c) HA conc. 5 mg/L, at lower contact time (5 - 25 min)

Table 4.6 Kinetic parameters of HA degradation by ZnO photocatalyst at various initial HA concentration

Co	UV-A			UV-C		
	K'	R ²	t _{1/2}	K'	R ²	t _{1/2}
5	0.065	0.750	10.73	0.062	0.855	11.21
8	0.046	0.728	15.16	0.030	0.923	23.33
11	0.028	0.936	24.75	0.028	0.962	24.66
14	0.022	0.923	31.64	0.020	0.976	34.65

4.3.1 Half-life (t_{1/2})

The computations of the half-life ($t_{1/2}$) for TiO₂ and ZnO are shown in Table 4.5 and 4.6, respectively. The shorter $t_{1/2}$ values indicate that the efficiency of the degradation process is higher. The $t_{1/2}$ values behave inversely with that of the K' values as expected as shown in Figure 4.19. From K' values comparison, it is

previously shown that ZnO performs better in UV-A irradiation while TiO₂ in UV-C irradiation. ZnO has lower $t_{1/2}$ values in UV-A irradiation which indicates higher efficiency than that of TiO₂ under UV-A conditions. On the other hand, TiO₂ has lower $t_{1/2}$ values in UV-C irradiation which indicates higher efficiency than that of ZnO under UV-C conditions. Rajamanickam et al. (2012) reported that the duration increased with increasing concentration of the solute. Furthermore he indicated that the intermediate decomposition products compete with the novel solute for the photo generated radical oxidizing species.

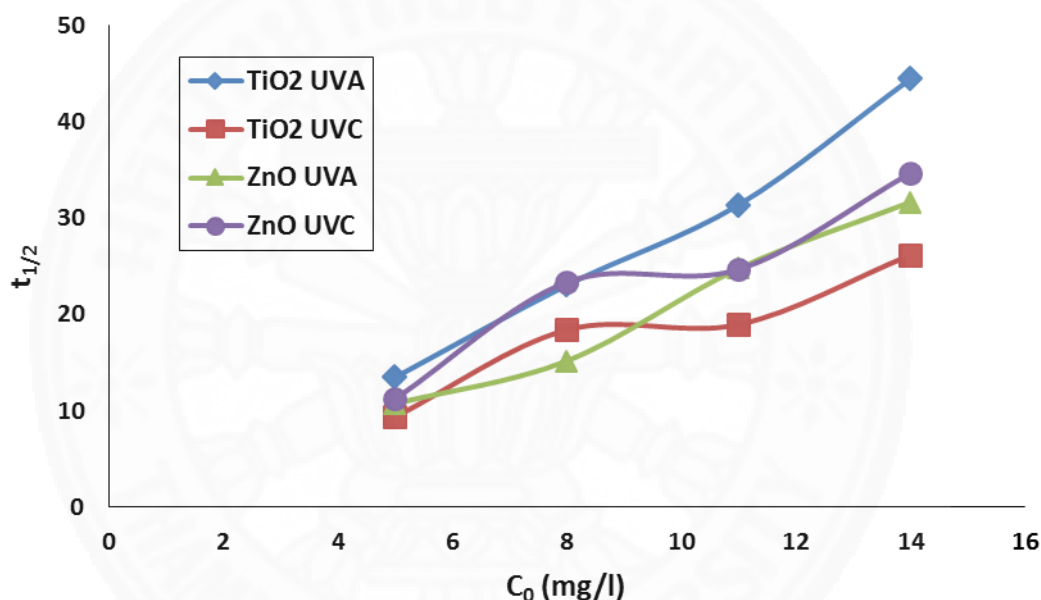


Figure 4.19 Half-life of L-H kinetic of HA photocatalytic degradation

4.3.2 Total Organic Carbon (TOC) and Mineralization

Throughout the experiments, total organic carbon was measured at optimum condition (HA conc. 14 mg/L, catalyst dose 0.3 g/L, contact time 180 min). Total organic carbon is the amount of carbon bound in an organic compound. This measurement can be used as an indicator for monitoring oxidation-reduction reactions of HA. The percentage of TOC degradation efficiency under UV-A and UV-C irradiations are shown in Table 4.7. The TOC analysis was observed from liquid and

solid phase. From the TOC solid phase results showed that the TOC value is very low, less than 1% for each catalyst.

Under UV-A irradiation, the degradation of TOC were 68% and 67% for TiO₂ and ZnO, respectively. However, under UV-C irradiation, the degradation efficiency decreased 49% and 21% for TiO₂ and ZnO, respectively. When comparing the TOC degradation efficiency with the HA degradation efficiency, the HA degradation efficiency was reached 90% at 180 min under UV-A and UV-C irradiations for TiO₂ and ZnO, which is much higher than the TOC degradation efficiency. It shows that the intermediate compounds were generated subsequent to the oxidation process, and incomplete mineralization of HA to the end product in form of CO₂ occurred. Referring to chemical structure of HA that mentioned on chapter 2, mostly chemical structure of HA is a carboxylic acids. Previous study reported that carboxylic acids are easily transformed into CO₂ and H₂O and the final carboxylic acid by product is oxalic acid (HOOC-COOH) (Yadollah et al., 2011). The residual TOC efficiency of mineralization specifies the presence of other photoproducts such as carboxylic acids at the termination of the reaction. It is evident that the photomineralization process of HA can be described by two key stages. In the first stage, there is a fragmentation of the macromolecules in tiny molecules with a gradual conversion of organic carbon in mineral carbon. In the second stage, these tiny molecules will re-adsorb at the catalyst surface and mineralize rapidly.

From the TOC analysis results in solid phase at 14 mg/L of HA concentration, 0.3 g/L of catalyst dose within 180 min in dark condition, it was found that the values for ZnO and TiO₂ cases were 0.09769 mg C/g and 0.082031 mg C/g, respectively. These results can be supported by the adsorption values obtained previously. The experimental results of adsorption process which were described previously in section 4.1.3 and 4.2.3 indicated that adsorption is the initial step of photodegradation. This can be supported by TOC results. The tested results in section 4.2.3 proved the expected outcome which is, higher adsorption in TiO₂ results in lower than the remaining organic carbon inside catalyst. For ZnO case in section 4.1.3, lower adsorption results in higher than the remaining carbon inside catalyst. The organic

carbon was found to be higher on solid catalyst after the adsorption, but the amount decreased after photodegradation for both cases of catalysts. It proves that adsorption acts as the initial step which is followed by photodegradation in terms of degrading the HA.

Table 4.7 The percentage of TOC degradation efficiency

Parameter	TOC Results			% Mineralization
	Liquid Phase (mg/L)	Solid Phase		
		%	(mg C/g)	
Initial	6.425	-	-	-
TiO ₂ UV-A	2.063	0.1037	0.0098	68%
TiO ₂ UV-C	3.116	0.5321	0.0787	49%
ZnO UV-A	2.052	0.7010	0.0694	67%
ZnO UV-C	5.015	0.4684	0.0299	21%

Chapter 5

Conclusions and Recommendations

5.1 Conclusions

Based on the experiments conducted in the present study for photocatalytic degradation of HA by using TiO₂ and ZnO photocatalyst, under UV-A and UV-C irradiations, the following conclusions can be drawn:

5.1.1 HA Degradation by ZnO Photocatalyst

- Degradation efficiencies under UV-A irradiation was higher than that of UV-C due to the highest illumination intensities of UV-C.
- The degradation efficiency was nearly consistent as the ZnO dose increases, for both irradiations at 5 mg/L of HA concentration.
- The HA degradation was constant with contact time, at 5 mg/L for both irradiations and continuously increasing at 14 mg/L.
- Degradation efficiency is increased with the increase of light intensity for all the tested cases. This is due to the fact that more radiation is absorbed by the catalyst surface for producing electron-hole pairs. This results in producing higher radical's which lead to higher degradation efficiency.
- In terms of adsorption isotherm, the process is dominated by photodegradation than that of adsorption process.
- Three cycles of reusability is suggested to be acceptable from the experiments from this study.

5.1.2 HA Degradation by TiO₂ Photocatalyst

- Degradation efficiencies under UV-C irradiation was higher than that of UV-A due to the fact that under lower dose of TiO₂, UV-A irradiation is less powerful to generate the hydroxyl radicals which can degrade HA.

- The degradation efficiency under UV-C was nearly consistent as the TiO₂ dose increases. However, For the case of UV-A irradiation, the degradation efficiency was considerably low at lower dosage of TiO₂ due to similar reason mentioned above.
- The HA degradation was constant with contact time, at 5 mg/L for both irradiations and continuously increasing at 14 mg/L. UV-C irradiation showed higher performance in HA degradation than that of the UV-A case.
- For lower light intensities, UV-C lamp shows more efficiency in degradation of HA than that of UV-A. However, in higher light intensities, UV-A shows higher performance of HA degradation. This is due to the different activation amount of TiO₂ phases.
- In terms of adsorption isotherm, the process is dominated by adsorption than that of photodegradation process.
- Five cycles of reusability is suggested to be acceptable from the experiments from this study.

5.1.3 Comparison of ZnO and TiO₂ Photocatalyst

- From FT-IR spectra results, it was found a new peak of by-products of HA appeared.
- From BET results, it was concluded that agglomeration of the catalyst was occurred after photocatalytic process for both photocatalysts.
- From XRF results, it was found that certain elements of by-products of HA were attached on the surface of catalyst.
- ZnO photocatalyst proved to be more compatible with UV-A light, whereas, TiO₂ with UV-C.
- In terms of the HA degradation efficiency, ZnO had higher HA degradation efficiency compared to TiO₂. In the short contact time 30 min to 60 min, it was reached more than 90%.

- In terms of light intensity, it proved that under low intensity lamp, HA can be successfully degraded in low range concentration of HA.
- In terms of catalyst reusability, for both catalysts are quite reusable. However, TiO₂ showed better photochemical stability than ZnO. From the cycles of the reuse, TiO₂ can be reused and still applicable until 5 cycles, whereas, ZnO only 3 cycles.
- From kinetics Langmuir-Hinshelwood, the first order kinetics expression can be successfully applied to investigate the photocatalytic reaction process. The correlation coefficients obtained for both TiO₂ and ZnO catalysts indicate good fitting of experimental data to that of the kinetics equation. And for both catalysts was indicated follows a pseudo first order kinetic expression.
- From TOC results, it was indicated that the mineralization process was not completely occurred, for both catalysts. It was found the amount of carbon remained from liquid phase and solid phase of samples. This indicated that the intermediate compounds were formed after the oxidation process, and incomplete mineralization of HA to the end product in form of CO₂ occurred.
- Based on TOC results, it can be concluded that the adsorption acts as the initial step which is followed by photodegradation in terms of degrading the HA

5.2 Recommendations

In order to improve the potential of photocatalytic process to degrade HA and other complex organic compounds in field applications, the following recommendations for future research are made as follows:

1. In the practical application, this treatment can be a good alternative to degrade HA. Due to the short contact time required to degrade HA in low

concentration range. Usually, HA concentration appear in natural water resources around 2 mg/L to 15 mg/L.

2. Since of ZnO is easily to agglomerate in the solution, ultrasonic pre-treatment required.
3. Since the energy levels take a part of this photocatalytic process, determine of energy levels is required in-depth of research.
4. Immobilization of the catalyst on various substrate will enhance the photocatalytic reaction and avoid the post separation difficulties with the powder form of catalyst, when concerns in practical application.
5. For this research, main concern was only for drinking water treatment process. The photocatalytic technology used in drinking water treatment has two key considerations for applying in practical applications, whether to be used as a pre-treatment step or stand-alone step. Pre-treatment is carried out to enhance biodegradation of organic pollutants before treatment and is an efficient method for HA. If used as a stand-alone step, need to increase the resident time until reach the complete mineralization.

References

- Adams, Laura K., Delina Y. Lyon, and Pedro J.j. Alvarez. (2006). Comparative Ecotoxicity of Nanoscale TiO₂, SiO₂, and ZnO Water Suspensions. *Water Research* 40: 3527-532.
- Akpan, U.G. and Hameed, B.H. 2011. Photocatalytic degradation of 2,4 dichlorophenoxyacetic acid by Ca-Ce-WTiO₂ composite photocatalyst. *Chemical Engineering Journal*. 173, 369-375
- Andayani, Winarti, and Agustin Bagyo. (2011).TiO₂ Beads for Photocatalytic Degradation of Humic Acid in Peat Water .*Indo. J. Chem.*, 2011, 11 (3): 253 - 257
- Bak S, Song M, Nam I, Lee WG, “Photocatalytic Oxidation of Trichloroethylene in Water Using a Porous Ball of Nano-ZnO and Nanoclay Composite”, *Journal of Nanomaterials*, Article ID 160212, 8 pages, (2015)
- Bekbolet, M., Suphandag, A.S. and Uyguner, C.S. 2001. An investigation of the photocatalytic efficiencies of TiO₂ powder on the decolourisation of humic acids. *Journal of Photochemistry and Photobiology A: Chemistry*. 148, 121-128
- B.R. Eggins, F.L. Palmer, J.A. Byrne, “Photocatalytic Treatment of Humic Substance in Drinking Water” in *Water Res.* 31, pp. 1223, 1997.
- Cid, Lucía D. C., María D. C. Grande, Eduardo O. Acosta, and Berta Ginzberg. (2012). Removal of Cr(VI) and Humic Acid by Heterogeneous Photocatalysis in a Laboratory Reactor and a Pilot Reactor. *Industrial & Engineering Chemistry Research* 51.28: 9468-474.
- D. Wuilloud et al., “Trace humic and fulvic acid determination in natural water by cloud point extraction/pre-concentration using non-ionic and cationic surfactants with FI-UV detection” , in *The Analyst*: 128, pp. 453-458, 2003.
- Dong, Changlong, Wei Chen, Cheng Liu, Yu Liu, and Haicheng Liu. (2014).Synthesis of Magnetic Chitosan Nanoparticle and Its Adsorption Property for Humic Acid from Aqueous Solution. *Colloids and Surfaces A: Physicochemical and Engineering Aspects* : 179-89.
- Erhayem, Mohamed, and Mary Sohn. (2014). Effect of Humic Acid Source on Humic Acid Adsorption onto Titanium Dioxide Nanoparticles. *Science of The Total Environment* 470-471 : 92-98.
- G.E. Fryxell, G. Cao, *Environmental Applications of Nanomaterials: Synthesis, Sorbents and Sensors*, World Scientific, (2007)

- Gaffney, Jeffrey, Nancy A. Marley, and Sue B. Clark. (1996). *Humic and Fulvic Acids and Organic Colloidal Materials in the Environment*.
- Gaya, U.I., Abdullah, A.H., “Heterogeneous photocatalytic degradation of organic contaminants over titanium dioxide: a review of fundamentals, progress and problems”, in *J. Photochem. Photobiol. C: Photochem. Rev.* 9, pp. 1-12, 2008.
- Getkaew Pansamut, Tawatchai Charinpanitkul and Achariya Suriyawong. (2013). *Removal of Humic Acid by Photocatalytic Process: Effect of Light Intensity*. Department of Chemical Engineering, Faculty of Engineering, Chulalongkorn University, Bangkok 10330, Thailand
- Gonzalez M.G., M.E. Conti, R.M. Palma, N.M. Arrigo: Dynamics of humic components and microbial activity under no-tillage or reduced tillage, as compared with native pasture (Pampa Argentina). *Biol. Fert. Soils* 39: 135ñ 138, 2003.
- H. Yang, G. Li, T. An, Y. Gao, and J. Fu, “Photocatalytic degradation kinetics and mechanism of environmental pharmaceuticals in aqueous suspension of TiO₂: a case of sulfa drugs,” *Catalysis Today*, vol. 153, no. 3-4, pp. 200–207, (2010)
- Hepplewhite C, Newcombe G and Knappe D, “NOM and MIB, who wins in the competition for activated carbon adsorption sites?”, in *Water Sci. Technol.* 49, pp. 257-267, (2004)
- International Humic Substance Society. 2013, <http://www.humicsubstances.org>
- J. Wiszniewski, D. Robert, J. Surmacz-Gorska, K. Miksch, and J.-V. Weber, “Photocatalytic decomposition of humic acids on TiO₂ Part I: Discussion of adsorption and mechanism,” *J. Photochem. Photobiol.*, vol. 152, pp. 267-273, 2002.
- Kavurmaci, Sibel Sen, and Miray Bekbolet. (2013). Photocatalytic Degradation of Humic Acid in the Presence of Montmorillonite. *Applied Clay Science* 75-76 : 60-66.
- Kinniburgh, D. G., van Riemsdijk, W. H., Koopal, L. K., Borkovec, M., Benedetti, M. F. and Avena, M. J., 1999, Ion binding to natural organic matter: competition, heterogeneity, stoichiometry and thermodynamic consistency, *Colloids Surfaces A-Physicochem. Engineer. Aspects* 151:147–166.
- Kim, J.K., Alajmy, J., Borges, A.C., Joo, J.C., Anh, H., and Campos, L.C, “Degradation of Humic Acid by Photocatalytic Reaction Using Nano-sized ZnO/Laponite Composite”, *Water Air Soil Pollut.* 224:1749, (2013)

- Kumakiri, Izumi, Spyros Diplas, Christian Simon, and Pawel Nowak. (2011) Photocatalytic Membrane Contactors for Water Treatment. *Industrial & Engineering Chemistry Research* 50.10 : 6000-008.
- Kumar, Harish, and Renu Rani. "Structural and Optical Characterization of ZnO Nanoparticles Synthesized by Microemulsion Route", *International Letters of Chemistry Physics and Astronomy*, 2013.
- L.Huang, F.Peng, H.Yu and H.Wang, *Solid State Sci.*11: 129–138, (2009)
- Lee, Hyunjoo, and Wonyong Choi.(2002) Photocatalytic Oxidation of Arsenite in TiO₂ Suspension: Kinetics and Mechanisms. *Environ. Sci. Technol.* 36 : 3872-878
- Lee, Soo-Ah, Kwang-Ho Choo, Chung-Hak Lee, Ho-In Lee, Taegwhan Hyeon, Wonyong Choi, and Heock-Hoi Kwon.(2001). Use of Ultrafiltration Membranes for the Separation of TiO₂ Photocatalysts in Drinking Water Treatment. *Ind. Eng. Chem. Res.* 40 : 1712-719
- Liu, Sanly, May Lim, and Rose Amal. (2014).TiO₂-coated Natural Zeolite: Rapid Humic Acid Adsorption and Effective Photocatalytic Regeneration. *Chemical Engineering Science* 105 : 46-52.
- Liu, Sanly, May Lim, Rolando Fabris, Christoper Chow, Mary Drikas, and Rose Amal. (2008). TiO₂ Photocatalysis of Natural Organic Matter in Surface Water: Impact on Trihalomethane and Haloacetic Acid Formation Potential. *Environ. Sci. Technol.* 42: 6218-223.
- Lowe, J., and Md.m. Hossain. (2008). Application of Ultrafiltration Membranes for Removal of Humic Acid from Drinking Water. *Desalination* 218.1-3 : 343-54.
- Ma H, Wallis LK, Diamond S, Li S, Canas-Carrell J, Parra A (2014) Impact of solar UV radiation on toxicity of ZnO nanoparticles through photocatalytic reactive oxygen species (ROS) generation and photo-induced dissolution. *Environ Pollut* 193:165–172
- Manoj A. Lazar, Shaji Varghese and Santhosh S. Nair. (2012). Photocatalytic Water Treatment by Titanium Dioxide: Recent Updates.
- Meng Nan Chong, Bo Jin, Christopher W.K. Chow and Chris Saint. (2010). Recent developments in photocatalytic water treatment technology: A review
- Oskoei, V., M.H. Dehghani, S. Nazmara, B. Heibati, M. Asif, I. Tyagi, Shilpi Agarwal, and Vinod Kumar Gupta. "Removal of humic acid from aqueous solution using UV/ZnO nano-photocatalysis and adsorption", *Journal of Molecular Liquids*, 2016

- Palmer, F., Eggins, B., Coleman, H., "The effect of operational parameters on the photocatalytic degradation of humic acid", in *J. Photochem. Photobiol. Chem.* 148, pp. 137-143, 2002.
- Qin, Hongchun, Weiyang Li, Yujing Xia, and Tao He. (2011). Photocatalytic Activity of Heterostructures Based on ZnO and N-Doped ZnO. *ACS Applied Materials & Interfaces* 3.8 : 3152-156.
- Ravichandrika, K., Kiranmayi, P. & Ravikumar, (2012). Synthesis, characterization and antibacterial activity of ZnO nanoparticles, *International Journal of pharmacy and pharmaceutical Science*, 4, ISSN-0975-1491, p. 336-338.
- Richard T. Lamar, Daniel C. Olk, Lawrence Mayhew and Paul R. Bloom. (2014). A New Standardized Method for Quantification of Humic and Fulvic Acids in Humic Ores and Commercial Product.
- Romão, Joana, David Barata, Pamela Habibovic, Guido Mul, and Jonas Baltrusaitis. (2014) . High Throughput Analysis of Photocatalytic Water Purification. : 7612-617
- S. Mohammad, N. Maryam, B. Shahram, "Nano TiO₂ as an efficient and reusable heterogeneous catalyst for the synthesis of 5-substituted 1H-tetrazoles", *Journal of Natural Sciences Research* Vol.1, No.3, 2011.
- Sekartaji, Putri Ardyarini and Sandhya Babel. Degradation of humic acid by using TiO₂ photocatalyst. In *Proceedings of the 10th GMSARN International Conference 2015 on Smart Energy, Environment and Community Development in GMS*, (2015)
- Setyawati, L.M., 1994, Symposium of Peat Water Treatment, Palangkaraya.
- Tipping, E., 2002. Cation binding by humic substances. *Cambridge Environmental Chemistry Series* 12.
- T.A.AL- Dhahir. (2013). Quantitative Phase Analysis for Titanium Dioxide From X-Ray Powder Diffraction Data Using The Rietveld Method. *Physics Department , University of Baghdad*
- Thamaphat, K., Limsuwan, P. and Ngotawornchai, B, "Phase Transition of TiO₂ Powder by XRD and TEM", in *Kasetsart Journal (Natural Science)*, 42, pp. 357-361, 2008.
- Tashauoei, H. R., H. Movahedian Attar, M. M. Amin, M. Kamali, M. Nikaeen, and M. Vahid Dastjerdi. (2010). Removal of Cadmium and Humic Acid from Aqueous Solutions Using Surface Modified Nanozeolite A. *International Journal of Environmental Science & Technology* 7.3 : 497-508.

- Wallace, Brian. (2003). TOC Analysis of Humic Acid: Sample Preparation Is the Key.
- Wang, Jiahong, Lijuan Bi, Yanfen Ji, Hongrui Ma, and Xiaolong Yin. (2014). Removal of Humic Acid from Aqueous Solution by Magnetically Separable Polyaniline: Adsorption Behavior and Mechanism. *Journal of Colloid and Interface Science* : 140-46.
- Wang, Wendong, Wen Wang, Qinghai Fan, Yabo Wang, Zixia Qiao and Xiaochang Wang . (2014). Effects of UV Radiation on Humic Acid Coagulation Characteristics in Drinking Water Treatment Processes. *Chemical Engineering Journal* 256 : 137-43.
- Wu, Yanpeng, Wenming Zhang, Chongfang Ma, Yuanwei Lu, and Li Liu. (2010). Photocatalytic Degradation of Formaldehyde by Diffuser of Solar Light Pipe Coated with Nanometer Titanium Dioxide Thin Films. *Science in China Series E: Technological Sciences* 53.1 : 150-54.
- Yang, Jae-Kyu, and Seung-Mok Lee. (2006). Removal of Cr(VI) and Humic Acid by Using TiO₂ Photocatalysis. *Chemosphere* 63.10 : 1677-684.
- Yustiawati et al. *Environ Sci Pollut Res* (2015) 22: 2384. Effects of peat fires on the characteristics of humic acid extracted from peat soil in Central Kalimantan, Indonesia
- Zhang, Xian, Panyue Zhang, Zhen Wu, Ling Zhang, Guangming Zeng, and Chunjiao Zhou. (2013). Adsorption of Methylene Blue onto Humic Acid-coated Fe₃O₄ Nanoparticles. *Colloids and Surfaces A: Physicochemical and Engineering Aspects* 435: 85-90.
- Zulfikar, M. A., E. Novita, R. Hertadi, and S. D. Djajanti. (2013). Removal of Humic Acid from Peat Water Using Untreated Powdered Eggshell as a Low Cost Adsorbent. *International Journal of Environmental Science and Technology* 10.6 : 1357-366.



Appendices

Appendix A

Properties of HA-Sodium Salt

SIGMA-ALDRICH

ALDRICH
Chemistry

Riedstrasse 2, D-89555 Steinheim/Germany
Tel: +49 73 2997 2550 Fax: +49 73 2997 2557

Certificate of Analysis

Product Name: HUMIC ACID SODIUM SALT
technical grade
Product Number: H16752
Product Brand: Aldrich
Molecular Formula:
Molecular Mass:
CAS Number: 68131-04-4

TEST	SPECIFICATION	LOT STBB1688V RESULTS
APPEARANCE (COLOR)	BLACK	BLACK
APPEARANCE (FORM)	GRANULES	GRANULES
ALUMINIUM (ICP)		3.84 %
BARIUM (ICP)		0.0086 %
CALCIUM (ICP)		0.809 %
CHROMIUM (ICP)		0.0058 %
COPPER (ICP)		0.0044 %
IRON (ICP)		0.976 %
GALLIUM (ICP)		0.0010 %
POTASSIUM (ICP)		0.17 %
LITHIUM (ICP)		0.0023 %
MAGNESIUM (ICP)		0.100 %
MANGANESE (ICP)		0.0020 %
SODIUM (ICP)		5.99 %
SILICON (ICP)		4.77 %
STRONTIUM (ICP)		0.0060 %
TITANIUM (ICP)		0.438 %
VANADIUM (ICP)		0.0114 %
ZIRCONIUM (ICP)		0.0109 %
QC RELEASE DATE	02/DEC/09	

Appendix B

HA Standard

B.1 Humic Acid Methodology

Procedure for determining humic acid content

STANDARD STOCK PREPARATION (1000 ppm)

Dry Humic Acid (I.H.S.S.) for 4 hours @ 105 degrees centigrade. Weigh out 0.1075 g of Humic Acid and dilute to 100 ml with deionized (DI) water. Shake for 1 hour.

STANDARD PREPARATION

Take 5 ml of Humic Acid Standard Stock Solution and dilute to 100ml with DI water to make 50 ppm standard solution. Take 10 ml and dilute to 100 ml to make 100 ppm standard. Take 20 ml and dilute to 100ml to make 200 ppm standard.

TEST PROCEDURE

With Spectrophotometer set at 450 nm, set up standard curve with the 50, 100 and 200 ppm standards, using water as a blank. Read your sample and calculate concentration from the standard curve.

CALCULATIONS

(ppm Humic Acid from standard curve) x (dilution factor) = ppm Humic Acid
% Humic Acid = ppm Humic Acid / 10,000

DTPA = Diethylenetriamine Penta Acetic Acid

HPTA Method - Please note that the Humic Products Trade Association, in conjunction with the International Humic Substance Society (IHSS) is developing a new and much improved testing method for humic acid. The method detection limits for HA and FA were 4.62 and 4.8 mg/L, respectively. The method quantitation limits for HA and FA were 14.7 and 15.3 mg/L, respectively.

B.2 Humic Acid Standard Curve

Concentration(mg/l)	(Abs)
0	0
5	0.144
10	0.275
15	0.391
20	0.538
25	0.669

Appendix C

Pertinent factors of HA degradation (ZnO)

C.1 Effect of HA concentration

Initial concentration (mg/L)	Initial absorbance	Final absorbance	Final concentration (mg/L)	% removal
UV-A				
0	0	0	0	0
5	0.144	0.006	0.223880597	95.52238806
8	0.214	0.035	1.305970149	83.67537313
11	0.295	0.102	3.805970149	65.40027137
14	0.375	0.183	6.828358209	51.22601279
UV-C				
0	0	0	0	0
5	0.144	0.003	0.111940299	97.76119403
8	0.214	0.055	2.052238806	74.34701493
11	0.295	0.116	4.328358209	60.65128901
14	0.375	0.196	7.313432836	47.76119403

C.2 Effect of ZnO dose

Initial concentration (mg/L)	TiO ₂ Concentration (g/L)	Initial absorbance	Final absorbance	Final concentration (mg/L)	% removal
UV-A					
5	0.1	0.144	0.006	0.22	95.52
	0.3		0.005	0.19	96.27
	0.5		0.005	0.19	96.27
	0.8		0.002	0.07	98.51
	1		0.008	0.30	94.03
UV-C					
5	0.1	0.144	0.003	0.11	97.76
	0.3		0.004	0.15	97.01
	0.5		0.002	0.07	98.51
	0.8		0.003	0.11	97.76
	1		0.006	0.22	95.52

C.3 Effect of Contact time

Initial concentration (mg/L)	Contact time (min)	Initial absorbance	Final absorbance	Final concentration (mg/L)	% removal
UV-A					
5	30	0.144	0.006	0.22	95.52
	60		0.005	0.19	96.27
	90		0.003	0.11	97.76
	120		0.004	0.15	97.01
	150		0.002	0.07	98.51
	180		0.012	0.45	91.04
UV-C					
5	30	0.144	0.009	0.34	93.28
	60		0.005	0.19	96.27
	90		0.006	0.22	95.52
	120		0.007	0.26	94.78
	150		0.004	0.15	97.01
	180		0.012	0.45	91.04

Initial concentration (mg/L)	Contact time (min)	Initial absorbance	Final absorbance	Final concentration (mg/L)	% removal
UV-A					
14	30	0.375	0.195	7.28	48.03
	60		0.125	4.66	66.68
	90		0.063	2.35	83.21
	120		0.013	0.49	96.54
	150		0.026	0.97	93.07
	180		0.006	0.22	98.40
UV-C					
14	30	0.375	0.203	7.57	45.90
	60		0.085	3.17	77.35
	90		0.082	3.06	78.14
	120		0.005	0.19	98.67
	150		0.015	0.56	96.00
	180		0.012	0.45	96.80

C.4 Effect of Light Intensity

Initial concentration (mg/L)	Contact time (min)	Initial absorbance	Final absorbance	Final concentration (mg/L)	% removal
UV-A					
UV-A (0.131 mw/cm ²)					
14	30	0.375	0.195	7.28	48.03
	60		0.125	4.66	66.68
	90		0.063	2.35	83.21
	120		0.013	0.49	96.54
	150		0.026	0.97	93.07
	180		0.009	0.34	97.60
UV-C					
UV-C (0.196 mw/cm ²)					
14	30	0.375	0.203	7.57	45.90
	60		0.085	3.17	77.35
	90		0.056	2.09	85.07
	120		0.005	0.19	98.67
	150		0.015	0.56	96.00
	180		0.012	0.45	96.80

Initial concentration (mg/L)	Contact time (min)	Initial absorbance	Final absorbance	Final concentration (mg/L)	% removal
UV-A					
UV-A (0.167 mw/cm ²)					
14	30	0.375	0.158	5.90	57.89
	60		0.016	0.60	95.74
	90		0.011	0.41	97.07
	120		0.013	0.49	96.54
	150		0.012	0.45	96.80
	180		0.008	0.30	97.87
UV-C					
UV-C (0.233 mw/cm ²)					
14	30	0.375	0.220	8.21	41.36
	60		0.079	2.95	78.94
	90		0.018	0.67	95.20
	120		0.010	0.37	97.33
	150		0.012	0.45	96.80
	180		0.008	0.30	97.87

Initial concentration (mg/L)	Contact time (min)	Initial absorbance	Final absorbance	Final concentration (mg/L)	% removal
UV-A					
UV-A (0.236 mw/cm ²)					
14	30	0.375	0.153	5.71	59.22
	60		0.012	0.45	96.80
	90		0.009	0.34	97.60
	120		0.011	0.41	97.07
	150		0.008	0.30	97.87
	180		0	0.00	100.00
UV-C					
UV-C (0.284 mw/cm ²)					
14	30	0.375	0.218	8.13	41.90
	60		0.064	2.39	82.94
	90		0.015	0.56	96.00
	120		0.006	0.22	98.40
	150		0.007	0.26	98.13
	180		0.002	0.07	99.47

Appendix D

Pertinent factors of HA degradation (TiO₂)

D.1 Effect of HA concentration

Initial concentration (mg/L)	Initial absorbance	Final absorbance	Final concentration (mg/L)	% removal
UV-A				
0	0	0	0	0
5	0.144	0.035	1.305970149	73.88059701
8	0.214	0.069	2.574626866	67.81716418
11	0.295	0.153	5.708955224	48.10040706
14	0.375	0.199	7.425373134	46.96162047
UV-C				
0	0	0	0	0
5	0.144	0.005	0.186567164	96.26865672
8	0.214	0.016	0.597014925	92.53731343
11	0.295	0.077	2.873134328	73.88059701
14	0.375	0.156	5.820895522	58.42217484

D.2 Effect of TiO₂ dose

Initial concentration (mg/L)	TiO ₂ Concentration (g/L)	Initial absorbance	Final absorbance	Final concentration (mg/L)	% removal
UV-A					
5	0.1	0.144	0.035	1.31	73.88
	0.3		0.006	0.22	95.5
	0.5		0.006	0.22	95.5
	0.8		0.013	0.49	90.3
	1		0.008	0.30	94.0
UV-C					
5	0.1	0.144	0.005	0.19	96.3
	0.3		0.003	0.11	97.8
	0.5		0.004	0.15	97.0
	0.8		0.006	0.22	95.5
	1		0.004	0.15	97.0

D.3 Effect of Contact time

Initial concentration (mg/L)	Contact time (minute)	Initial absorbance	Final absorbance	Final concentration (mg/L)	% removal
UV-A					
5	30	0.144	0.008	0.30	94.0
	60		0.006	0.22	95.5
	90		0.002	0.07	98.5
	120		0.009	0.34	93.3
	150		0.013	0.49	90.3
	180		0.004	0.15	97.0
UV-C					
5	30	0.144	0.004	0.15	97.0
	60		0.003	0.11	97.8
	90		0	0.00	100.0
	120		0.002	0.07	98.5
	150		0.009	0.34	93.3
	180		0.004	0.15	97.0

Initial concentration (mg/L)	Contact time (min)	Initial absorbance	Final absorbance	Final concentration (mg/L)	% removal
UV-A					
14	30	0.375	0.131	4.89	65.1
	60		0.127	4.74	66.2
	90		0.089	3.32	76.3
	120		0.068	2.54	81.9
	150		0.043	1.60	88.5
	180		0.021	0.78	94.4
UV-C					
14	30	0.375	0.117	4.37	68.8
	60		0.097	3.62	74.1
	90		0.035	1.31	90.7
	120		0.023	0.86	93.9
	150		0.005	0.19	98.7
	180		0.007	0.26	98.1

D.4 Effect of Light Intensity

Initial concentration (mg/L)	Contact time (min)	Initial absorbance	Final absorbance	Final concentration (mg/L)	% removal
UV-A (0.131 mw/cm ²)					
14	30	0.375	0.131	4.89	65.1
	60		0.127	4.74	66.2
	90		0.089	3.32	76.3
	120		0.068	2.54	81.9
	150		0.043	1.60	88.5
	180		0.021	0.78	94.4
UV-C (0.196 mw/cm ²)					
14	30	0.375	0.117	4.37	68.8
	60		0.097	3.62	74.1
	90		0.035	1.31	90.7
	120		0.023	0.86	93.9
	150		0.005	0.19	98.7
	180		0.007	0.26	98.1

Initial concentration (mg/L)	Contact time (min)	Initial absorbance	Final absorbance	Final concentration (mg/L)	% removal
UV-A (0.167 mw/cm ²)					
14	30	0.375	0.112	4.18	70.1
	60		0.089	3.32	76.3
	90		0.042	1.57	88.8
	120		0.019	0.71	94.9
	150		0.003	0.11	99.2
	180		0	0.00	100.0
UV-C (0.233 mw/cm ²)					
14	30	0.375	0.093	3.47	75.2
	60		0.053	1.98	85.9
	90		0.029	1.08	92.3
	120		0.014	0.52	96.3
	150		0	0.00	100.0
	180		0	0.00	100.0

Initial concentration (mg/L)	Contact time (min)	Initial absorbance	Final absorbance	Final concentration (mg/L)	% removal
UV-A (0.236 mw/cm ²)					
14	30	0.375	0.071	2.65	81.1
	60		0.020	0.75	94.7
	90		0.012	0.45	96.8
	120		0.006	0.22	98.4
	150		0.005	0.19	98.7
	180		0	0.00	100.0
UV-C (0.284 mw/cm ²)					
14	30	0.375	0.085	3.17	77.3
	60		0.033	1.23	91.2
	90		0.018	0.67	95.2
	120		0.005	0.19	98.7
	150		0	0.00	100.0
	180		0	0.00	100.0

Appendix E

Reusability of Catalyst

E.1 ZnO

UV-A	% Catalyst recovery	% Catalyst Lost	Final absorbance	Final concentration (mg/L)	% removal
Initial					100
recovery 1	100	0	0.02	0.75	94.7
recovery 2	88	12	0.024	0.90	93.6
recovery 3	86.2	13.8	0.044	1.64	88.3

UV-C	% Catalyst recovery	% Catalyst Lost	Final absorbance	Final concentration (mg/L)	% removal
Initial					99.5
recovery 1	100	0	0.049	1.83	86.9
recovery 2	85	15	0.084	3.13	77.6
recovery 3	81.8	18.2	0.09	3.36	76.0

E.2 TiO₂

UV-A	% Catalyst recovery	% Catalyst Lost	Final absorbance	Final concentration (mg/L)	% removal
Initial					100
recovery 1	100	0	0.002	0.07	99.5
recovery 2	88	12	0.06	2.24	84.0
recovery 3	86.2	13.8	0.07	2.61	81.3
recovery 4	85	15	0.086	3.21	77.1
recovery 5	84.1	15.9	0.098	3.66	73.9

UV-C	% Catalyst recovery	% Catalyst Lost	Final absorbance	Final concentration (mg/L)	% removal
Initial					100
recovery 1	100	0	0.002	0.07	99.5
recovery 2	85	15	0.086	3.21	77.1
recovery 3	81.8	18.2	0.097	3.62	74.1
recovery 4	79.9	20.1	0.128	4.78	65.9
recovery 5	78.4	21.6	0.162	6.04	56.8

Appendix F

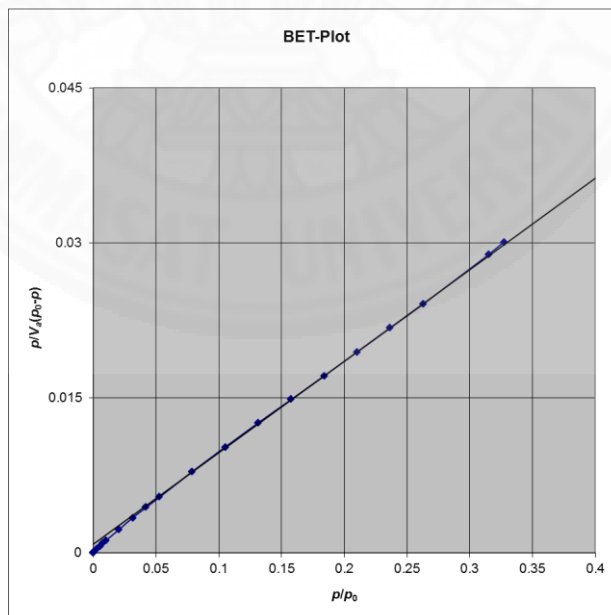
BET Analysis Results

F.1 ZnO

File Name	ZnO2 UV-A.DAT
Date of measurement	23/01/2059
Time of measurement	4:50:28
COMMENT 1	port1
COMMENT 2	tirapote
COMMENT 3	150C-overnight
COMMENT 4	port1, Vacuum degree before measurement:4.236E-1Pa
Serial number	BELmax 00092
Version	

Sample weight	3.88E-02 [g]	Saturated vapor pressure	102.49 [kPa]
Standard volume	24.236 [cm ³]	Adsorption cross section area	0.162 [nm ²]
Dead volume	18.6 [cm ³]	File name of walladsorption	
Equilibrium time	0 [sec]	Wall adsorption correction value 1	
Adsorptive	N2	Wall adsorption correction value 2	
Apparatus temperature	0 [C]	Number of adsorption data	23
Adsorption temperature	77 [K]	Number of desorption data	0

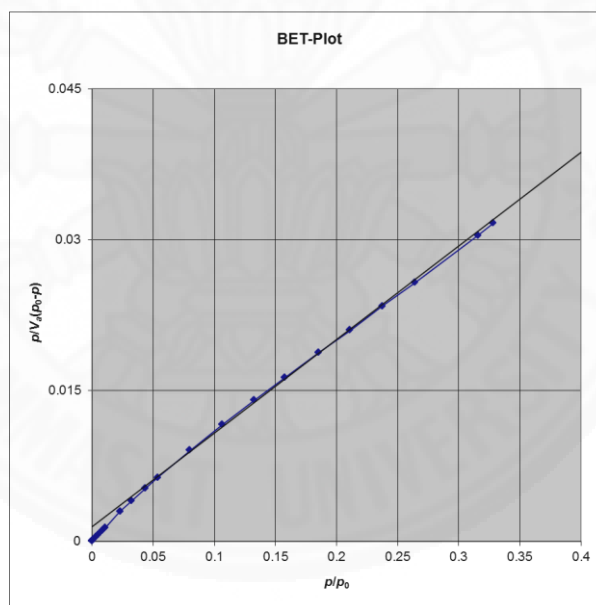
Starting point	13
End point	20
Slope	0.088484
Intercept	0.00087996
Correlation coefficient	0.9999
Vm	11.19 [cm ³ (STP) g ⁻¹]
a _s BET	48.705 [m ² g ⁻¹]
C	101.55
Total pore volume (p/p ₀ =0.327)	0.024998 [cm ³ g ⁻¹]
Average pore diameter	2.053 [nm]



File Name	ZnO2 UV-C.DAT
Date of measurement	23/01/2059
Time of measurement	4:31:02
COMMENT1	port3
COMMENT2	tirapote
COMMENT3	150C-overnight
COMMENT4	port3, Vacuum degree before measurement:4.236E-1Pa
Serial number	BELmax 00092
Version	

Sample weight	4.50E-02 [g]	Saturated vapor pressure	102.59 [kPa]
Standard volume	24.236 [cm ³]	Adsorption cross section area	0.162 [nm ²]
Dead volume	28.37 [cm ³]	File name of walladsorption	
Equilibrium time	0 [sec]	Wall adsorption correction value 1	
Adsorptive	N2	Wall adsorption correction value 2	
Apparatus temperature	0 [C]	Number of adsorption data	22
Adsorption temperature	77 [K]	Number of desorption data	0

Starting point	11
End point	19
Slope	0.093037
Intercept	0.0014787
Correlation coefficient	0.9996
Vm	10.58 [cm ³ (STP) g ⁻¹]
a _{s,BET}	46.05 [m ² g ⁻¹]
C	63.919
Total pore volume (p/p ₀ =0.328)	0.023843 [cm ³ g ⁻¹]
Average pore diameter	2.0711 [nm]

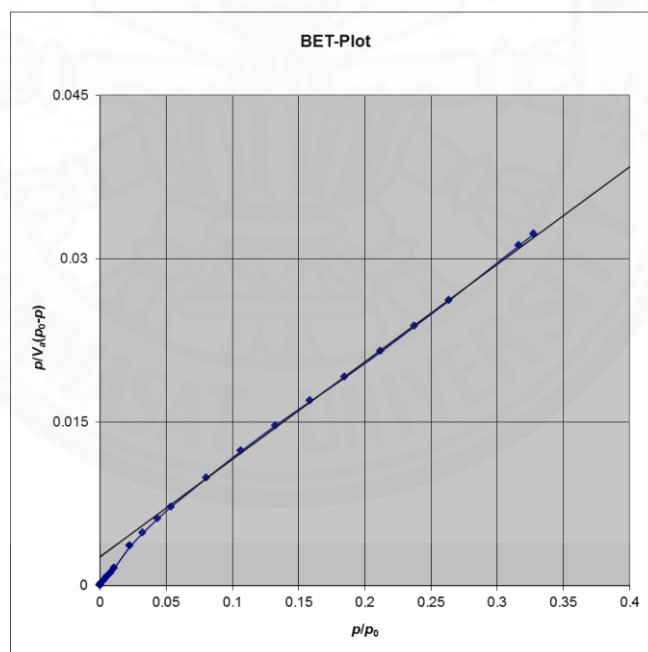


F.2 TiO₂

File Name	TiO2 UV-A.DAT
Date of measurement	20/01/2059
Time of measurement	4:20:43
COMMENT1	port3
COMMENT2	Fang
COMMENT3	150 degree C 3 h
COMMENT4	port3, Vacuum degree before measurement:4.261E-1Pa
Serial number	BELmax 00092
Version	

Sample weight	2.64E-02 [g]	Saturated vapor pressure	102.04 [kPa]
Standard volume	24.236 [cm ³]	Adsorption cross section area	0.162 [nm ²]
Dead volume	28.435 [cm ³]	File name of walladsorption	
Equilibrium time	0 [sec]	Wall adsorption correction value 1	
Adsorptive	N2	Wall adsorption correction value 2	
Apparatus temperature	0 [C]	Number of adsorption data	22
Adsorption temperature	77 [K]	Number of desorption data	0

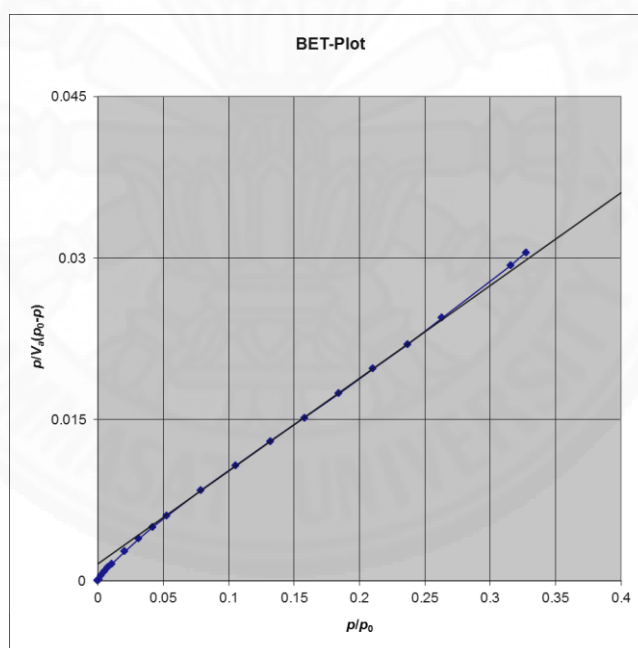
Starting point	12
End point	18
Slope	0.08936
Intercept	0.0026674
Correlation coefficient	0.9995
Vm	10.866 [cm ³ (STP) g ⁻¹]
a _{s,BET}	47.296 [m ² g ⁻¹]
C	34.5
Total pore volume (p/p ₀ =0.328)	0.023335 [cm ³ g ⁻¹]
Average pore diameter	1.9735 [nm]



File Name	TiO2 UV-C.DAT
Date of measurement	22/01/2059
Time of measurement	4:23:34
COMMENT1	port1
COMMENT2	tirapote
COMMENT3	150C-overnight
COMMENT4	port1, Vacuum degree before measurement:4.316E-1Pa
Serial number	BELmax 00092
Version	

Sample weight	1.99E-02 [g]	Saturated vapor pressure	102.21 [kPa]
Standard volume	24.236 [cm ³]	Adsorption cross section area	0.162 [nm ²]
Dead volume	18.256 [cm ³]	File name of walladsorption	
Equilibrium time	0 [sec]	Wall adsorption correction value 1	
Adsorptive	N2	Wall adsorption correction value 2	
Apparatus temperature	0 [C]	Number of adsorption data	21
Adsorption temperature	77 [K]	Number of desorption data	0

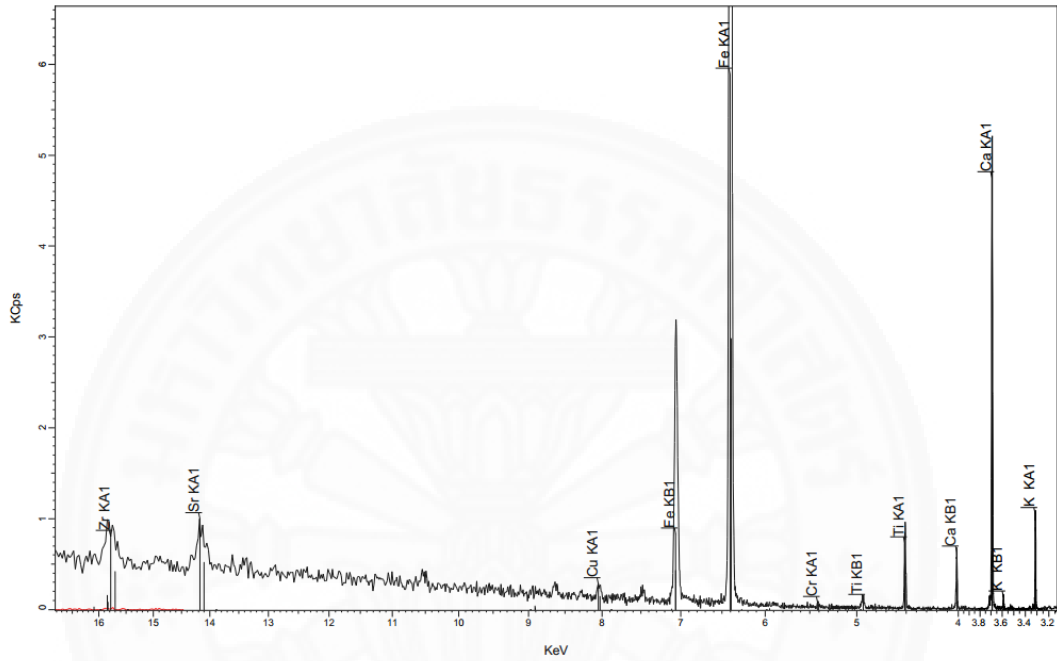
Starting point	11
End point	18
Slope	0.086194
Intercept	0.0015842
Correlation coefficient	1
Vm	11.392 [cm ³ (STP) g ⁻¹]
a _{s,BET}	49.585 [m ² g ⁻¹]
C	55.408
Total pore volume (p/p ₀ =0.327)	0.024662 [cm ³ g ⁻¹]
Average pore diameter	1.9895 [nm]



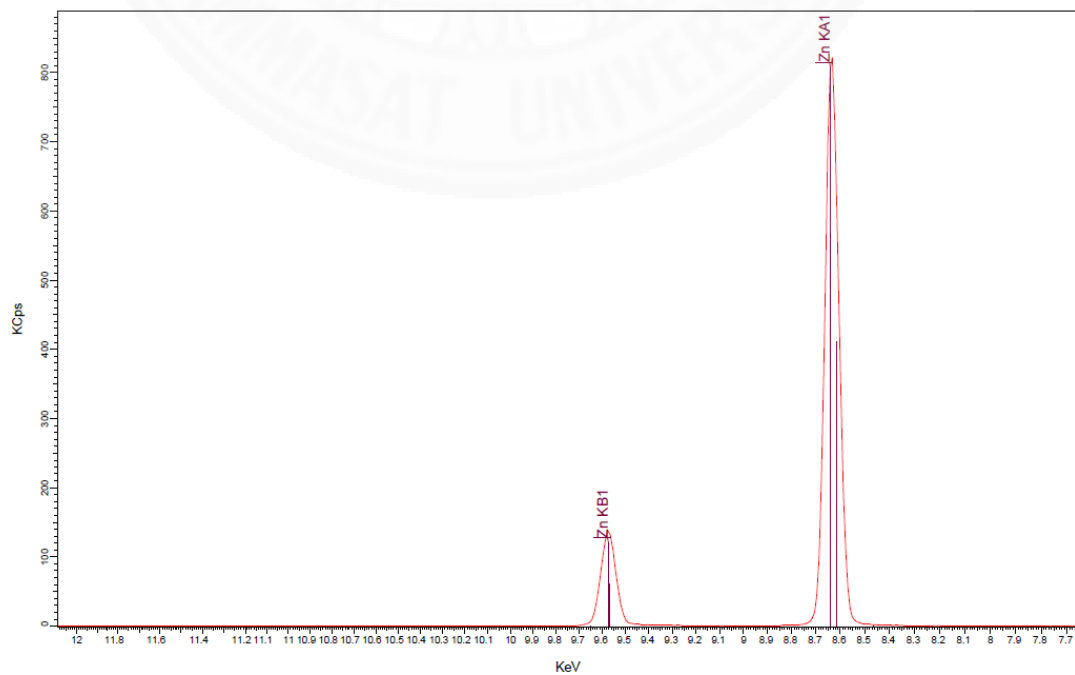
Appendix G

XRF Analysis Results

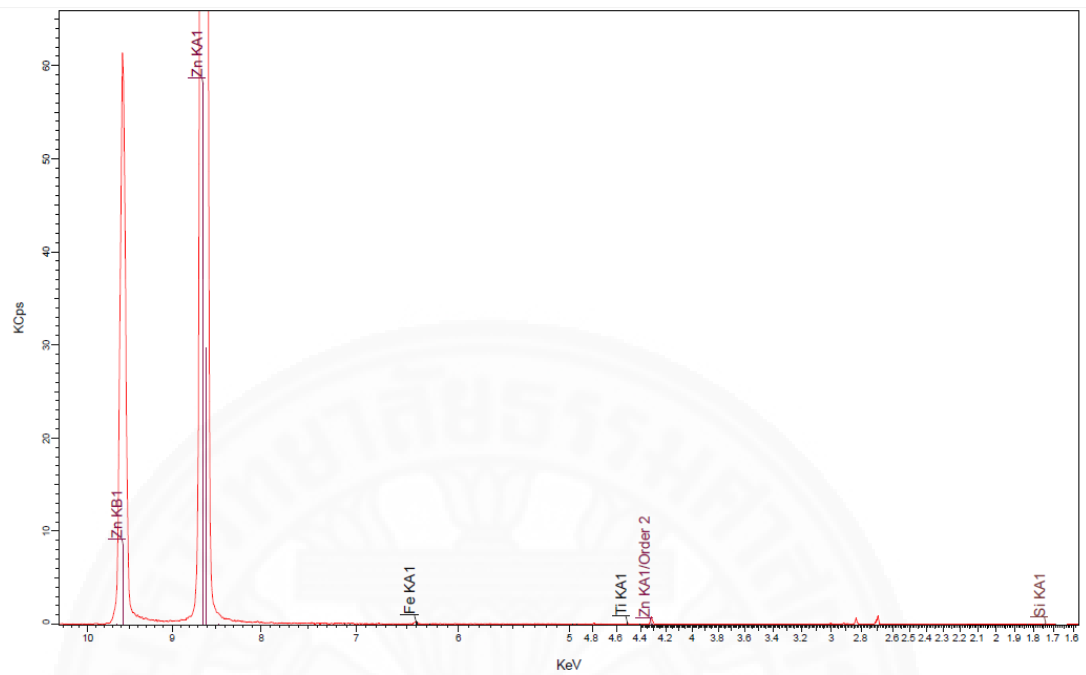
G.1 Initial Humic Acid



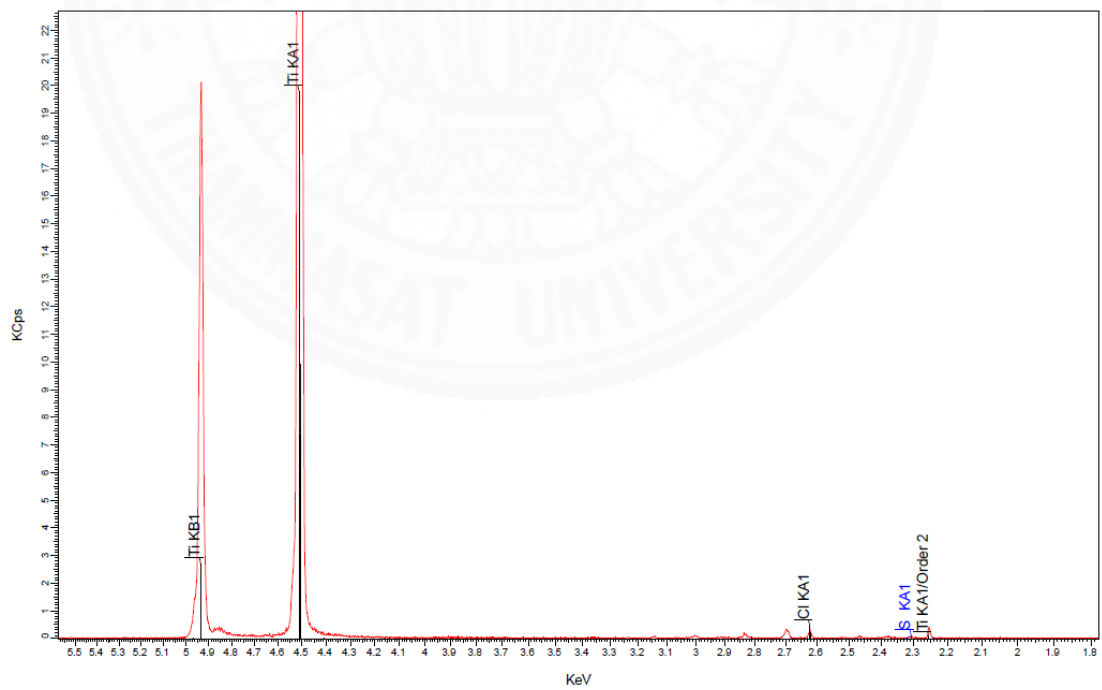
G.2 Initial ZnO



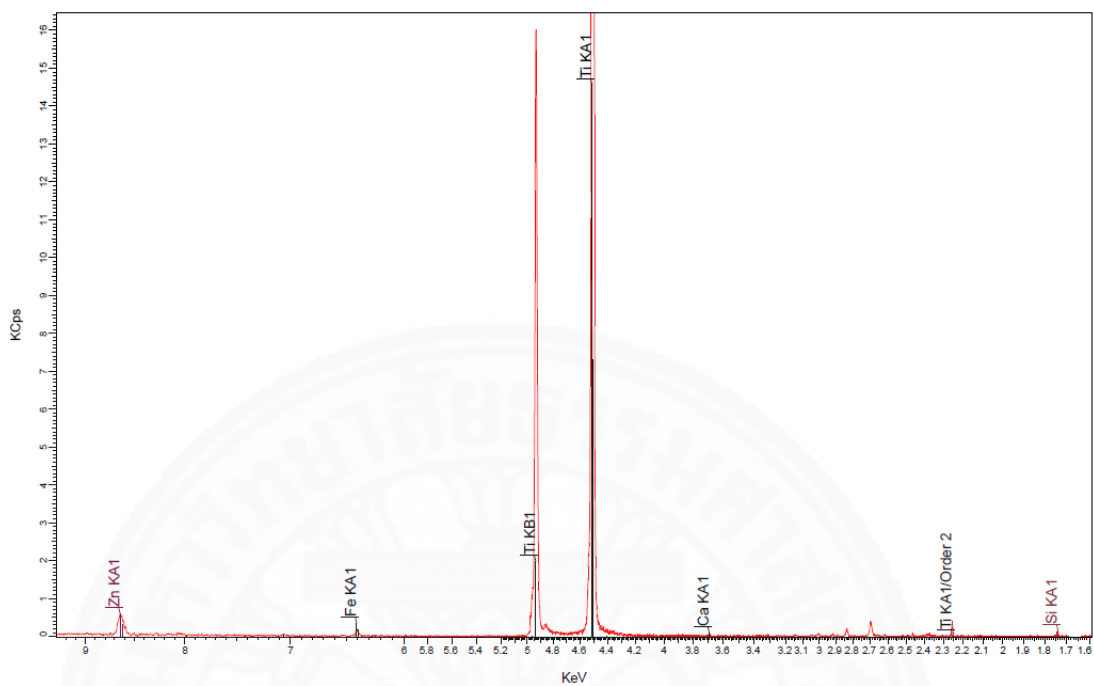
G.3 ZnO UV-A



G.4 Initial TiO₂



G.5 TiO₂ UV-C



Appendix H

Diffuse reflectance UV-vis spectroscopy Results

